*Burns & Trauma*, 2026, 14, tkag040
https://doi.org/10.1093/burnst/tkag040
Published: 5 June 2026
**Research Article**

OXFORD

# Adipose-derived stem cell peptide 5 alleviates hypertrophic scarring through targeting pyruvate carboxylase or p50 to coordinate PI3K/AKT/mTOR-autophagy and NF-κB/IL-6 signaling

**Ling Chen[1,2], Enyuan Zhang[1], Siqi Zeng[1], Qiyue Yan[1], Jingyun Li[3], Qian Li[1], Jun Li[1,*], Zezhang Zhu[2,*]**

[1]Department of Plastic&Cosmetic Surgery, Women's Hospital of Nanjing Medical University (Nanjing Women and Children's Healthcare Hospital), 123 Tianfei Street, Mochou Road, Nanjing 210004, China
[2]Division of Spine Surgery, Department of Orthopedic Surgery, Nanjing Drum Tower Hospital, Affiliated Hospital of Medical School, Nanjing University, 321 Zhongshan Road, Nanjing 210008, China
[3]Nanjing Women and Children's Healthcare Institute, Women's Hospital of Nanjing Medical University (Nanjing Women and Children's Healthcare Hospital), 123 Tianfei Street, Mochou Road, Nanjing 210004, China
*Corresponding authors. Zezhang Zhu, E-mail: zhuzezhang@126.com; Jun Li, E-mail: drlijun123@163.com.

## Abstract

***Background:*** **Hypertrophic scars are a major clinical challenge with limited treatments. Adipose-derived stem cells (ADSCs) play an important role in inhibiting pathological scar formation. However, the underlying mechanisms remain unclear. In this study, we aimed to investigate the function, mechanism, and therapeutic potential of adipose-derived stem cell peptide 5 (ADSCP5), a novel peptide from adipose-derived stem cell-conditioned medium.**

***Methods:*** **We used *in vitro* hypertrophic scar fibroblast, macrophage–fibroblast coculture and human umbilical vein endothelial cell (HUVEC) assays, RNA sequencing, pathway analysis, peptide pull-down, molecular docking, cellular thermal shift assays, surface plasmon resonance, immunofluorescence colocalization analysis, western blotting, rescue experiments, reactive oxygen species (ROS), autophagy tests, and mitochondrial membrane potential assays and untargeted metabolomics. The efficacy of ADSCP5 was validated in rabbit and porcine scar models.**

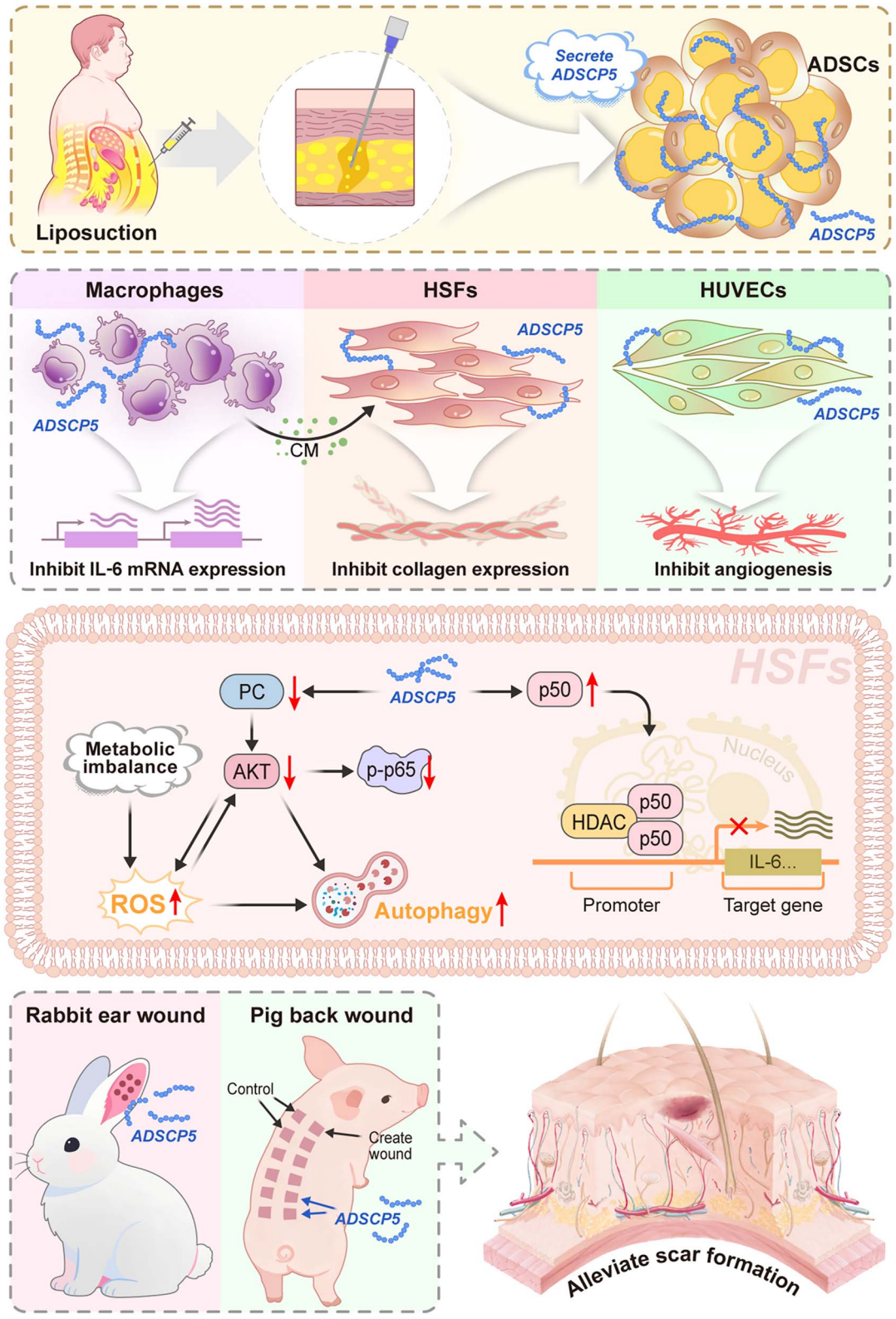
***Results:*** **In hypertrophic scar fibroblasts, ADSCP5 significantly downregulated the expression of collagen genes (COL1A1, COL1A2, and COL3A1) and actin alpha 2, smooth muscle, without affecting cell proliferation, apoptosis, or migration. Transcriptomic, enrichment, and western blot analyses confirmed that ADSCP5 reduced the protein levels of phosphorylated p65 (p-p65, NF-κB subunit), p-PI3K, p-AKT, and p-mTOR. Moreover, ADSCP5 decreased IL-6 transcription. Mechanistically, ADSCP5 bound directly to pyruvate carboxylase or the NF-κB subunit p50. This interaction resulted in the downregulation of PC or the upregulation of p50, ultimately inhibiting collagen expression, a finding confirmed by rescue assays. Furthermore, ADSCP5 induced ROS generation and autophagy, altered global metabolism, and modulated macrophage–fibroblast crosstalk to suppress fibrosis. It also exhibited antiangiogenic effects in HUVECs. In both the rabbit and porcine scar models, ADSCP5 treatment effectively attenuated collagen deposition and scar hyperplasia, increased the number of macrophages (increased CD68), reduced angiogenesis (decreased VEGFA and CD34), and promoted autophagy (reduced p62).**

***Conclusions:*** **Overall, this study demonstrate that ADSCP5 alleviates hypertrophic scarring by directly binding to PC and p50, suppressing the PI3K/AKT/mTOR and NF-κB pathways, reducing IL-6 and collagen production, promoting ROS and autophagy, and modulating metabolic, macrophage and angiogenic responses. These findings position ADSCP5 as a promising therapeutic agent for hypertrophic scar prevention and treatment.**

**Received:** 13 November 2025. **Revised:** 20 May 2026. **Accepted:** 2 June 2026
© The Author(s) 2026. Published by Oxford University Press.
This is an Open Access article distributed under the terms of the Creative Commons Attribution-NonCommercial License (https://creativecommons.org/licenses/by-nc/4.0/), which permits non-commercial re-use, distribution, and reproduction in any medium, provided the original work is properly cited. For commercial re-use, please contact reprints@oup.com for reprints and translation rights for reprints. All other permissions can be obtained through our RightsLink service via the Permissions link on the article page on our site—for further information please contact journals.permissions@oup.com.

Downloaded from academic.oup.com/burnstrauma/article/doi/10.1093/burnst/tkag040/8702856 by guest on 12 October 2026

## Graphical abstract




**Keywords** Hypertrophic scar, ADSCP5, Fibroblasts, pyruvate carboxylase, p50, Scar treatment, Adipose-derived stem cells

Downloaded from academic.oup.com/burnstrauma/article/doi/10.1093/burnst/tkag040/8702856 by guest on 12 October 2026

## Highlights

- **Adipose-derived stem cells peptide 5 (ADSCP5), a novel peptide from adipose-derived stem cells, effectively alleviates hypertrophic scarring in rabbit and porcine models.**
- **Mechanistically, ADSCP5 directly binds to pyruvate carboxylase or the NF-$\kappa$B subunit p50.**
- **ADSCP5 inhibits the PI3K/AKT/mTOR and NF-$\kappa$B/IL-6 signaling pathways while inducing reactive oxygen species generation and autophagy.**
- **ADSCP5 suppresses collagen deposition by modulating macrophage-fibroblast crosstalk and anti-angiogenic effects.**

# Background

Hypertrophic scarring is a common pathological phenomenon during wound healing that significantly impairs functional recovery and quality of life [1]. Although various therapeutic approaches exist, their efficacy remains unsatisfactory [1]. Hypertrophic scarring is characterized primarily by excessive deposition of extracellular matrix in the dermis and is closely associated with postinjury tissue repair mechanisms involving inflammatory responses, fibroblast proliferation, collagen synthesis, angiogenesis, and tissue remodeling [2]. Enhanced expression of collagen type I (COL1A1 and COL1A2), collagen type III (COL3A1), and the myofibroblast marker gene ACTA2 (actin alpha 2 and smooth muscle) are hallmark features of hypertrophic scars [3]. Various signaling pathways, including TGF-$\beta$/SMAD, NF-$\kappa$B/IL-6, and PI3K/AKT/mTOR, have been reported to be involved in the regulation of hypertrophic scars [1, 4]. Despite substantial progress in elucidating the regulatory mechanisms of hypertrophic scars, the pursuit of an ideal therapy continues to represent a critical and unmet challenge.

In recent years, adipose-derived stem cells (ADSCs) have garnered considerable attention due to their paracrine functions in tissue repair and regeneration [5–7]. The ADSC secretome facilitates wound healing through several mechanisms: modulating macrophage phenotypic switching to influence the inflammatory phase; promoting angiogenesis by enhancing endothelial cell differentiation and migration; and mediating granulation tissue formation, skin cell regeneration, and extracellular matrix synthesis to advance the proliferative and remodeling phases [8]. However, the specific mechanisms underlying their role in suppressing hypertrophic scarring remain incompletely elucidated.

Peptide-based therapeutics hold great promise in disease treatment owing to their low molecular weight, high specificity, and low toxicity [9]. Multiple peptides inhibit scarring through diverse pathways [10]. Pro-healing peptide- and peptide-based interventions against skin wound healing have been extensively studied [11–15]. Our previous work demonstrated that the ADSC-derived peptide ADSCP2 inhibits hypertrophic scarring [16]. In the current study, we screened another functional peptide named adipose-derived stem cell peptide 5 (ADSCP5). Cellular functional assays demonstrated that ADSCP5 significantly suppressed the protein expression of type I collagen (COL1A1 and COL1A2) and the myofibroblast marker ACTA2 without significantly affecting cell proliferation, apoptosis, or migration. In rabbit and porcine scar models, ADSCP5 alleviated collagen deposition and hypertrophic scarring. Mechanistic analysis revealed that ADSCP5 alleviated hypertrophic scarring through targeting pyruvate carboxylase (PC) or p50 to coordinate PI3K/AKT/mTOR-autophagy and NF-$\kappa$B/IL-6 signaling. Overall, this study provides new theoretical insights and potential therapeutic agents for the prevention and treatment of pathological scarring.

# Methods

## Ethics statement

This study was approved by the Ethics Committee of Women's Hospital of Nanjing Medical University (Nanjing Women and Children's Healthcare Hospital) (2022KY-162). Human hypertrophic scar tissues were obtained with written informed consent from patients undergoing surgery.

## Identification, synthesis, and preparation of peptides

Our previous work identified a total of 1108 peptides in ADSC-CM obtained at 48 h [16]. Based on the mass spectrometry results, we selected ADSCP5 because of its conservation and potential functional roles. Peptides (purity $>$98%), including ADSCP5 (sequence: ADKPDMGEIASFDKAKLKKTETQEKN) and its scrambled control (Sc, sequence: AEKAKDQKFDKEDNGITTLKMSKPEA, which shares the same amino acid composition as ADSCP5 but in a random order, controlling for nonsequence-specific effects), were synthesized by Shanghai Peptide Biotechnology Co., Ltd and dissolved in sterile distilled water (15230162, Thermo Fisher Scientific). A biotin-labeled version was used for pull-down assays. FITC-labeled ADSCP5 was used for location analysis.

## Cell culture and treatment

Primary human hypertrophic scar fibroblasts (HSFs) [16] at passages 3–7 were maintained in Fibroblast Medium (2301, ScienCell). Cells were treated with ADSCP5 or Sc (25 $\mu$M) for 24–48 h. For rescue experiments, an NF-$\kappa$B inhibitor (10 nM; BAY 11–7082, MCE, USA) or an AKT activator (SC79, 40 $\mu$M, prepared in DMSO; T2274, TargetMOI, USA) was applied with or without ADSCP5 for 36 h. The cells were pretreated with the ROS scavenger NAC (N-acetylcysteine; HY-B0215, MedChemExpress) at 1 mM (dissolved in DMSO) for 2 h with or without ADSCP5 for another 36 h.

## Quantitative reverse transcription polymerase chain reaction

Total RNA was extracted (RC112–1, Vazyme, Nanjing, China), and cDNA was synthesized for qPCR (Q711–02, Vazyme, Nanjing, China) on an ABI Vii7 system. The gene expression levels of human COL1A1, COL1A2, COL3A1, and ACTA2 were normalized to that of GAPDH using primers from previous work [16]. To analyze macrophage activation-related markers, quantitative PCR was carried out to assess the expression levels of mouse CD86, TNF-$\alpha$, IL-6, CD204, Arg-1, iNOS, CD80, CD206, IL-1, IL-4, and IL-10. The sequences of primers used are listed in Table 1, with mouse Hprt employed as the endogenous control for normalization.

Downloaded from academic.oup.com/burnstrauma/article/doi/10.1093/burnst/tkag040/8702856 by guest on 12 October 2026

**Table 1** Primer sequences used for genes

| Gene | Forward sequence(5′ to 3′) | Reverse sequence(5′ to 3′) |
|---|---|---|
| CD86 | TGTTTCCGTGGAGACGCAAG | TTGAGCCTTTGTAAATGGGCA |
| TNF-a | CAGGCGGTGCCTATGTCTC | CGATCACCCCGAAGTTCAGTAG |
| IL-6 | CTGCAAGAGACTTCCATCCAG | AGTGGTATAGACAGGTCTGTTGG |
| CD204 | TGGAGGAGAGAATCGAAAGCA | CTGGACTGACGAAATCAAGGAA |
| Arg-1 | CTCCAAGCCAAAGTCCTTAGAG | AGGAGCTGTCATTAGGGACATC |
| CD80 | TGCTGCTGATTCGTCTTTCAC | GAGGAGAGTTGTAACGGCAAG |
| CD206 | GCTTCCGTCACCCTGTATGC | TCATCCGTGGTTCCATAGACC |
| IL-1 | GAAATGCCACCTTTTGACAGTG | TGGATGCTCTCATCAGGACAG |
| IL-4 | GGTCTCAACCCCCAGCTAGT | GCCGATGATCTCTCTCAAGTGAT |
| IL-10 | GCTCTTACTGACTGGCATGAG | CGCAGCTCTAGGAGCATGTG |
| iNOS | GTTCTCAGCCCAACAATACAAGA | GTGGACGGGTCGATGTCAC |
| Hprt | TCAGTCAACGGGGGACATAAA | GGGGCTGTACTGCTTAACCAG |

**Table 2** Used antibody in the western blot assay

| Name | Brand | Catalog number |
|---|---|---|
| COL1A1 | Abclonal | A1352 |
| COL1A2 | Proteintech | 14695–1-AP |
| COL3A1 | Proteintech | 22734–1-AP |
| ACTA2 | Proteintech | 14395–1-AP |
| GAPDH | Proteintech | 10494–1-AP |
| $\beta$-ACTIN | Proteintech | 66009–1-Ig |
| $\beta$-Tubulin | Servicebio | ZB15140-HRP-100 |
| PC | Proteintech | 16588–1-AP |
| NF-$\kappa$B p50 | CST | #13586 |
| AKT | CST | 4685S |
| $\alpha$-Tubulin | Proteintech | 11224–1-AP |
| p-AKT(Ser473) | CST | 4058 |
| NF-$\kappa$B p65 | Proteintech | 10745–1-AP |
| p-p65(Ser536) | CST | 3033S |
| PI3K | Proteintech | 60225–1-Ig |
| p-PI3K p85/p55 (Tyr467/Tyr199) | Zenbio | 341468 |
| p-mTOR (Ser2448) | 67 778–1-Ig | Proteintech |
| mTOR | ab134903 | Abcam |
| p62 | 66 184–1-Ig | Proteintech |
| LC3 | 14 600–1-AP | Proteintech |

## Western blot analysis

Proteins were extracted using radio immunoprecipitation assay (RIPA) lysis buffer (P0013B, Beyotime, Beijing, China), separated by SDS-polyacrylamide gel electrophoresis, transferred onto polyvinylidene difluoride membranes, and probed with antibodies (Table 2). The signals were detected by enhanced chemiluminescence (ECL; Millipore, USA) and quantified with ImageJ (National Institutes of Health, MD, USA).

## Cell viability analysis

Cell viability was measured by a cell counting kit-8 assay (CCK-8; A311–01, Vazyme, Nanjing, China). Fibroblasts (2000 cells/well) were treated with 25 $\mu$M ADSCP5, Sc, or vehicle control in sextuplicate. After treatment, the cells were incubated with CCK-8 for 1 h at 37°C, and absorbance was measured at 450 nm using a microplate reader (Molecular Devices, California, USA).

## Cell apoptosis analysis

After Annexin V-FITC/PI staining, apoptosis was assessed by flow cytometry (A211–01, Vazyme, Nanjing, China). Following a 24-h treatment with 25 $\mu$M Sc, ADSCP5, or the control ($n = 3$), the cells were processed by flow cytometry (Beckman Coulter, USA), and 10 000 events per sample were analyzed using Kaluza software.

## Wound healing assay

Cell migration was evaluated using a scratch assay. A wound was introduced into a confluent fibroblast monolayer, followed by treatment with 25 $\mu$M Sc, ADSCP5, or the control ($n = 3$) in serum-free medium. The wound area was imaged at the indicated time points and quantified by measuring the gap width with ImageJ.

## Transwell migration assay

A Transwell migration assay was performed by seeding treated, serum-starved cells (Control, 25 $\mu$M Sc, or ADSCP5) in the upper chamber, with 10% FBS medium as a chemoattractant below. Following incubation (24/48 h), the migrated cells were fixed, stained with crystal violet, and quantified by imaging and Optical density (OD) measurement at 590 nm after 33% acetic acid lysis.

## Transcriptome sequencing analysis

Transcriptome profiling was performed on hypertrophic scar fibroblasts treated in triplicate with 25 $\mu$M Sc or ADSCP5. Total RNA was extracted and sequenced on the Illumina NovaSeq 6000 platform (PE150) by Shanghai Bio Corporation. Differentially expressed genes (DEGs) were identified using a threshold of fold change $\geq 1.5$ or $\leq 0.67$ and $P < 0.05$. Functional enrichment analysis of the DEGs was conducted through Gene Ontology (GO) and Kyoto Encyclopedia of Genes and Genomes (KEGG) pathway assessments.

RNA from porcine scar tissues harvested from control or ADSCP5-treated wounds on Day 42 was similarly extracted and sequenced. DEGs were determined using the same criteria,

Downloaded from academic.oup.com/burnstrauma/article/doi/10.1093/burnst/tkag040/8702856 by guest on 12 October 2026

followed by GO and KEGG enrichment analyses. The top 30 enriched KEGG pathways were ranked by Q value (Fisher's exact test). Gene set enrichment analysis (GSEA) was carried out using BROAD GSEA software with default parameters (1000 permutations).

## Pulldown assay and silver staining

Biotin-labeled ADSCP5 (50 $\mu$g) was bound to Dynabeads™ M-280 Streptavidin (11205D, Invitrogen) and incubated with 2 mg of protein lysate from hypertrophic scar fibroblasts. A biotin-labeled scrambled peptide served as the negative control. After being washed, the bound proteins were separated by SDS–PAGE and visualized using a Pierce™ silver stain kit (24600, Thermo Fisher). Differential bands were excised for mass spectrometry identification.

## Surface plasmon resonance

The binding affinity of ADSCP5 to PC or p50 was assessed using surface plasmon resonance (SPR) on an OpenSPR system (Nicoya Lifesciences Inc.). Recombinant human PC or p50 protein was initially expressed in a prokaryotic system (*Escherichia coli*) by Genecreate. The PC or p50 protein (20 $\mu$g/ml) was then immobilized on a CM5 sensor chip (Cytiva). Subsequently, graded concentrations of ADSCP5 or p50 were sequentially delivered across the chip surface. The interaction analysis was carried out under the following conditions: an association phase of 120 s, a dissociation phase of 300 s, and a maintained flow rate of 30 $\beta$l/min throughout the run..

## Immunofluorescence staining

Hypertrophic scar fibroblasts were incubated with FITC-conjugated ADSCP5. Following fixation with formaldehyde, the expression of PC or p50 was detected via immunofluorescence staining. Cells were probed with a primary antibody against PC (16588–1-AP, Proteintech) or p50 (13586, CST) and subsequently with a goat anti-rabbit IgG secondary antibody (mp02764, Invitrogen). Finally, the nuclei were counterstained with DAPI (mp01306, Invitrogen), and images were acquired using a Leica STELLARIS STED microscope.

## Cellular thermal shift assay

After being incubated with ADSCP5 or the control for 2 h, cells were heated to various temperatures (37°C, 41°C, 45°C, 48°C, and 51°C). Cell lysates were then prepared by three freeze–thaw cycles in liquid nitrogen, followed by centrifugation. The pellets were boiled in loading buffer and subjected to western blot analysis.

## Preparation of conditioned medium from ADSCP5-treated macrophages and coculture with hypertrophic scar fibroblasts

RAW264.7 macrophages (Chinese Academy of Sciences, Shanghai, China) at passages 3–7 were cultured in DMEM supplemented with 10% FBS and 1% penicillin–streptomycin. At 60% confluence, the cells were treated with 25 $\mu$M ADSCP5 or Sc or control for 24 h. Conditioned medium (CM) was collected, centrifuged at 5000 $\times$ g (10 min, 4°C), and applied to HSFs to evaluate its effects on collagen expression.

## Tube formation assay

human umbilical vein endothelial cells (HUVECs; Chinese Academy of Sciences, Shanghai, China) at passages 3–7 were plated at $1 \times 10^4$ cells/well on Matrigel (356234, Corning)-coated plates. Following incubation, capillary-like structures were imaged (20×) between 6 and 18 h. Tube formation was quantified (length, area, loops, and nodes) in three random fields per well using ImageJ.

## ROS detection

ROS levels were assessed in treated cells using a specific fluorescent probe. Cells were stained with 10 $\mu$M probe for 30 min at 37°C in the dark, and fluorescence was measured microscopically and quantified with ImageJ. The mean fluorescence intensity per cell from 5 random fields and three independent experiments is shown.

## Mitochondrial membrane potential assay

The mitochondrial membrane potential in hypertrophic scar fibroblasts treated with 25 $\mu$M Sc, ADSCP5, or control for 36 h was evaluated using a JC-1 assay kit (C2006, Beyotime, China). Cells were stained according to the manufacturers' instructions and analyzed by confocal microscopy (Leica STELLARIS STED) and flow cytometry (Beckman Coulter). JC-1 aggregates (red, normal) and monomers (green, depolarized) were detected. The mean fluorescence intensity per cell from five random fields and three independent experiments is shown.

## Autophagic flux analysis

Autophagic flux was analyzed in fibroblasts transfected with the mCherry-EGFP-LC3B reporter plasmid. Following 24 h of treatment with the control, Sc, or ADSCP5, cells were imaged by confocal microscopy, with yellow ($mCherry^+/EGFP^+$) and red ($mCherry^+/EGFP^-$) puncta representing autophagosomes and autolysosomes, respectively. Autophagic activity was evaluated by quantifying its ratio. The mean fluorescence intensity per cell from 5 random fields and three independent experiments is shown.

## Plasmid and siRNA transfections

As previously reported [16], we utilized the same PC and vehicle control plasmids. Transfected complexes containing ~1 $\mu$g of plasmid and 2 $\mu$l of Lipo3000 were introduced into each well of 6-well plates in medium supplemented with either 25 $\mu$M scrambled control peptide or ADSCP5. Protein was collected 48 h later for evaluation.

The p50-targeting siRNA (si-p50) and its negative control were designed by RiboBio, with the si-p50 sequence being 5'-GTC ACT CTA ACG TAT GCA A-3′. siRNA transfection was performed using a riboFECT CP Transfection Kit (RiboBio) in accordance with the manufacturer's instructions.

Downloaded from academic.oup.com/burnstrauma/article/doi/10.1093/burnst/tkag040/8702856 by guest on 12 October 2026

## Untargeted metabolomics

Hypertrophic scar fibroblasts treated with 25 $\mu$M Sc or ADSCP5 for 36 h were subjected to untargeted metabolomic profiling (BGI, China) using LC–MS/MS (Q Exactive, Thermo Fisher) in both positive and negative ion modes. The data were processed with Compound Discoverer 3.1 and analyzed using metaX. Differentially abundant metabolites were filtered by fold change (fold change $>1.2$ or $<0.83$), VIP (variable importance in the projection) $\geq 1$, and $P < 0.05$. Pathway enrichment analysis was performed based on the KEGG results, with $P < 0.05$ considered to indicate statistical significance.

## Establishment of a hypertrophic scar model in rabbit ears

All procedures were approved by the Experimental Animal Care and Use Committee (FJABR2022062201) and complied with NIH guidelines. Six male New Zealand white rabbits weighing 2.5 kg underwent creation of six 1-cm diameter full-thickness skin defects per ear under anesthesia with isoflurane gas. From Day 14, the wounds were subcutaneously injected with Sc, ADSCP5 (200 $\mu$M, 100 $\mu$l), or the blank control every 7 days ($n = 4$ total). On Day 42, scar tissues were harvested for hematoxylin and eosin (HE) and Masson's trichrome staining after euthanasia.

## Establishment of a dorsal scar model in Bama mini-pigs

Following ethical approval (FJABR2022122901), a dorsal scar model was established in five female Bama mini-pigs weighing 14 kg by creating six $3 \times 3$ cm full-thickness skin wounds on each side under anesthesia with intramuscular injection of tiletamine–zolazepam (Telazol) at a dose of 4 mg/kg into the gluteal muscle. Beginning on Day 14, the wounds were subcutaneously injected with ADSCP5 (200 $\mu$M) or the control treatment every 7 days. Scar tissues harvested on Day 42 were analyzed by HE, Masson's trichrome, and Sirius red staining.

## Immunohistochemistry analysis

Tissue sections were deparaffinized, rehydrated, and subjected to antigen retrieval in EDTA buffer (pH 9.0) via microwave irradiation. After blocking endogenous peroxidase activity and nonspecific sites, the sections were incubated overnight at 4°C with primary antibodies against p62 (1:500, Servicebio, GB11531), VEGFA (1:500, Servicebio, GB15165), CD34 (1:500, Servicebio, GB15013), CD68 (1:400, Servicebio, GB113109), or CD206 (1:500, Servicebio, GB153497). Detection was performed with an HRP-conjugated secondary antibody and diaminobenzidine (DAB) development, followed by hematoxylin counterstaining, dehydration, and mounting.

## Statistical analysis

Statistical analysis was performed using GraphPad Prism 8.0 (San Diego, CA, USA). Data are presented as the mean $\pm$ standard deviation (SD) of at least three independent biological replicates for *in vitro* experiments, while the sample sizes for *in vivo* studies are indicated in the respective figure legends. For comparisons between two groups, an unpaired Student's *t* test was employed. For experiments involving a single variable with more than two groups, one-way analysis of variance (ANOVA) followed by Tukey's multiple comparisons test was used. For experiments involving two independent factors (treatment and time/temperature), two-way ANOVA followed by Sidak's or Tukey's multiple comparisons test was applied to evaluate the main effects and their interactions. A $P$ value $<0.05$ was considered to indicate statistical significance.

# Results

## ADSCP5 inhibited the mRNA and protein expression of collagen and alpha smooth muscle actin in human hypertrophic scar fibroblasts

Sequence analysis revealed that ADSCP5 was highly conserved across humans, mice, rats, rabbits, and pigs (Figure 1a; the red box indicates the position of ADSCP5). The secondary structure of ADSCP5 was predicted (Figure 1b) using the online tool PEP-FOLD3 [17]. The results of the mass spectrometry analysis of ADSCP5 are shown in Figure 1c.

As we previously reported [16], 25 $\mu$M ADSCP5 was added to the culture medium of human primary hypertrophic scar fibroblasts. For consistency and comparability, we directly adopted the same concentration of 25 $\mu$M in the present study. The results of the CCK-8 assay demonstrated that ADSCP5 did not significantly affect the proliferative activity of human primary hypertrophic scar fibroblasts (Figure 1d). The qPCR and western blot analyses revealed that ADSCP5 significantly inhibited the mRNA and protein expression levels of type I and III collagen, as well as the myofibroblast marker ACTA2, in human primary hypertrophic scar fibroblasts (Figure 1e, 1f). The results of apoptosis assays demonstrated that ADSCP5 had a minimal effect on apoptosis (Figure 1g). Scratch wound and Transwell assays were performed to evaluate the effect of ADSCP5 on cellular migration. The results demonstrated that ADSCP5 treatment did not significantly affect the migratory capacity of hypertrophic scar fibroblasts (Figure 1h, Supplemental Figure 1).

## ADSCP5 regulated NF-$\kappa$B and PI3K/AKT signaling

To elucidate the downstream mechanisms underlying the effects of ADSCP5, we performed RNA sequencing on hypertrophic scar fibroblasts treated with either the control Sc peptide or ADSCP5 (Figure 2a). Transcriptomic analysis revealed differential gene expression patterns, as shown in the volcano plot (Figure 2b). Compared with the control peptide, ADSCP5 treatment significantly upregulated the expression of 240 genes (fold change $\geq 1.50$, $P < 0.05$) and downregulated the expression of 243 genes (fold change $\leq 0.67$, $P < 0.05$) (Figure 2b). KEGG pathway enrichment analyses of these 483 differentially expressed genes revealed significant associations with the NF-$\kappa$B signaling pathway (Figure 2c). Further GSEA revealed that interferon-alpha, inflammatory response, cholesterol homeostasis, and

Downloaded from academic.oup.com/burnstrauma/article/doi/10.1093/burnst/tkag040/8702856 by guest on 12 October 2026

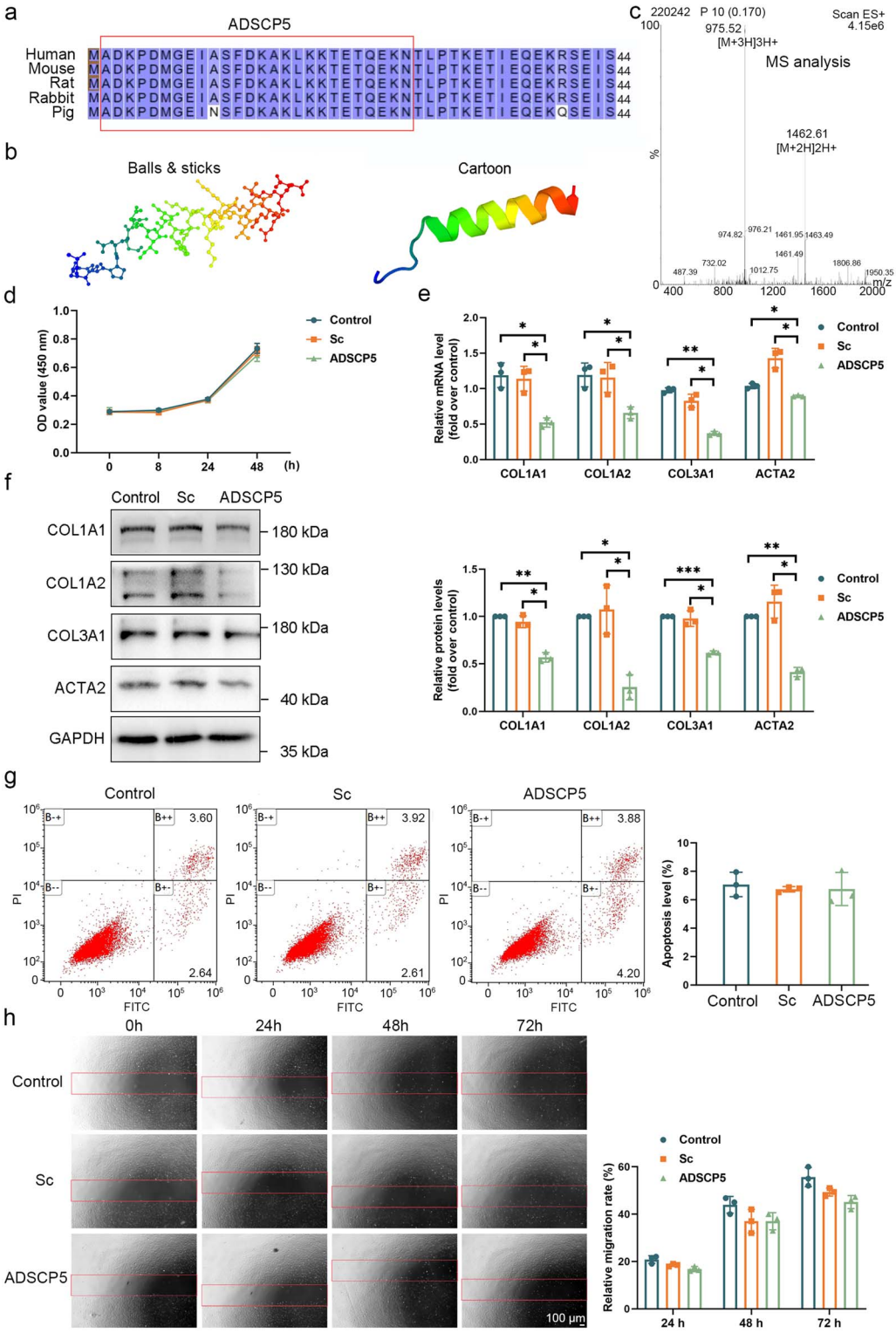



**Figure 1** Effects of ADSCP5 on collagen and ACTA2 expression in hypertrophic scar fibroblasts. (**a**) Conservation analysis of ADSCP5. (**b**) Secondary structure of ADSCP5. (**c**) Mass spectrometry analysis of ADSCP5. (**d**) CCK-8 testing revealed no significant alterations. (**e**) ADSCP5 inhibited the mRNA expression levels of collagens and ACTA2. (**f**) ADSCP5 decreased the protein expression levels of collagens and ACTA2. (**g**) The results of the apoptosis test revealed little change. (**h**) The results of the cell migration analysis revealed little change. Band intensities from western blot analyses were quantified using ImageJ software. Scale bar: 100 $\mu$m. The data are presented as the mean ± SD from three independent experiments. The protein expression level in the control group was normalized to 1. One-way ANOVA followed by Tukey's multiple comparisons test was used. $^{*}P < 0.05$, $^{**}P < 0.01$, $^{***}P < 0.001$. *ADSCP5* adipose-derived stem cell peptide 5, *Control* solvent control, *Sc* scrambled peptide control, *MS* Mass spectrometry, *OD* optical density, *COL1A1* collagen type I alpha 1 chain, *COL1A2* collagen type I alpha 2 chain, *COL3A1* collagen type III alpha 1 chain, *ACTA2* Actin alpha 2, *GAPDH* Glyceraldehyde-3-phosphate dehydrogenase, *PI* propidium iodide, *FTIC* fluorescein isothiocyanate

Downloaded from academic.oup.com/burnstrauma/article/doi/10.1093/burnst/tkag040/8702856 by guest on 12 October 2026

PI3K/AKT/mTOR signaling were enriched (Figure 2d). We then investigated the effects of ADSCP5 on the levels of p-p65, p65, p-PI3K, PI3K, p-AKT, AKT, p-mTOR, and mTOR in hypertrophic scar fibroblasts using western blotting. The results indicated that ADSCP5 decreased the protein levels of p-p65, p-PI3K, p-AKT and p-mTOR (Figure 2e, 2f). As a multifunctional cytokine, IL-6 is involved in various physiological processes, including inflammatory responses, immune regulation, and tissue repair. IL-6/p-STAT3 signaling has been shown to increase fibroblast proliferation and extracellular matrix production, underscoring its critical role in scar formation [18]. IL-6 is also downstream of NF-$\kappa$B and promotes scar hyperplasia [19]. We further examined changes in IL-6 expression in hypertrophic scar fibroblasts following ADSCP5 treatment. Treatment with 25 $\mu$M ADSCP5 for 48 h significantly reduced the transcription of IL-6 (Figure 2g). These findings suggest that the mechanisms of ADSCP5 involve multiple signaling pathways, including the NF-$\kappa$B/IL-6 and PI3K/AKT/mTOR signaling pathways.

## ADSCP5 bound to the PC and p50 proteins, downregulating AKT and upregulating p50 protein expression

To identify potential protein interactors of ADSCP5, we performed peptide pull-down assays followed by silver staining (Supplemental Figure 2a). The differentially stained protein bands were excised and subjected to mass spectrometry analysis. Mass spectrometry identified 73 differentially enriched proteins in the ADSCP5 group (the top 20 proteins are listed in Supplemental Figure 2b). Enrichment analysis of the mass spectrometry results revealed that the identified ADSCP5-binding proteins were primarily involved in biological processes, including the endocrine system, immune system, and signal transduction (Supplemental Figure 2c).

Among these identified proteins, the PC protein was previously recognized as an ADSCP2-binding partner in our earlier studies [16] and thus was selected as our primary target for further analysis. Concurrently, the p50 protein was also prioritized for investigation due to its established association with the NF-$\kappa$B pathway and its molecular weight corresponding to one of the differentially stained bands. Molecular docking analysis was subsequently performed for both proteins (Figure 3a). Using the HDOCK SERVER (http://hdock.phys.hust.edu.cn/), we obtained docking scores of −167.897 for the ADSCP5–PC complex and − 146.863 for the ADSCP5–p50 complex (Figure 3a), suggesting potential binding interactions between ADSCP5 and both the PC and p50 proteins.

We then performed western blot analysis to examine changes in PC and p50 protein expression following ADSCP5 treatment. The results demonstrated that compared with the control treatment, ADSCP5 treatment significantly downregulated PC but markedly upregulated p50 expression (Figure 3b). Furthermore, CETSA and SPR confirmed direct binding interactions between ADSCP5 and both the PC and p50 proteins (Figure 3c, 3d). FITC-labeled ADSCP5 could enter the cell membrane and was located mainly in the cytoplasm (Figure 3e). The results of the mass spectrometry analysis of FITC-labeled ADSCP5 are shown in Figure 3f. Immunofluorescence colocalization analysis revealed that ADSCP5 colocalized with PC and p50 (Figure 3g). Overexpression of PC reversed the effects of ADSCP5 on the protein levels of COL1A1 and COL1A2 (Figure 4a). In addition, knockdown of p50 reversed the effects of ADSCP5 on the protein level of COL1A1 (Figure 4a).

The p50 homodimer has been identified as a critical anti-inflammatory transcription factor that functions by suppressing proinflammatory gene expression while promoting anti-inflammatory gene expression. Hypertrophic scar fibroblasts were treated with 10 nM NF-$\kappa$B inhibitor (BAY 11–7082) and ADSCP5 for 36 h and compared with a control group. Western blot analysis revealed that the NF-$\kappa$B inhibitor could counteract the ADSCP5-mediated suppression of COL1A1, COL1A2, and COL3A1 protein expression in hypertrophic scar fibroblasts (Figure 4b). Furthermore, we examined whether the AKT activator SC79 could attenuate the inhibitory effects of ADSCP5 on these collagen proteins. Western blot results demonstrated that SC79 treatment similarly reversed the ADSCP5-induced downregulation of COL1A1, COL1A2, and COL3A1 protein expression (Figure 4c).

## ADSCP5 promoted reactive oxygen species production and autophagy and had mild effects on the mitochondrial membrane potential

According to the literature, inhibition of PC expression suppresses the synthesis of oxaloacetic acid, disrupts mitochondrial pyruvate metabolism, and increases oxidative stress [20]. Therefore, we treated HSFs with 25 $\mu$M ADSPC5. After 24 h, the levels of intracellular reactive oxygen species (ROS) were measured using an ROS assay kit. The results revealed that ADSCP5 promoted ROS production in hypertrophic scar fibroblasts (Figure 5a). PC localizes to the mitochondria and catalyzes the conversion of pyruvate to oxaloacetic acid, providing substrates for the mitochondrial tricarboxylic acid (TCA) cycle. Thus, we used JC-1 staining followed by fluorescence microscopy and flow cytometry to detect changes in the mitochondrial membrane potential. After treatment with ADSCP5, the ratio of red/green fluorescence decreased, indicating that the mitochondrial membrane potential had partially decreased (Figure 5b, 5c).

Our research group recently discovered that the AKT/mTOR pathway influences autophagy and plays a significant role in the process of scar hyperplasia [21]. Moreover, activation of the PI3K/AKT/mTOR pathway was reported to regulate hypertrophic scar formation by modulating autophagy [22]. Therefore, we treated HSFs with 25 $\mu$M ADSPC5. Experiments utilizing a dual-fluorescence reporter system (mCherry-GFP-LC3) for monitoring autophagic flux confirmed that ADSPC5 enhances the formation of autolysosomes and promotes autophagic flux (Figure 5d). The expression of autophagy-related proteins was assessed using western blot analysis. The results demonstrated that ADSPC5 significantly reduced the expression of p62 (Figure 5e), indicating the induction of autophagic flux. The ROS scavenger NAC reversed the effects of ADSCP5 on the protein level of COL1A1 (Figure 5f).

## Untargeted metabolomics to reveal the functions of ADSCP5

Given the crucial role of PC in anabolic processes, including gluconeogenesis, lipogenesis, insulin secretion, and glutamate neurotransmitter synthesis [23], decreased PC gene expression

Downloaded from academic.oup.com/burnstrauma/article/doi/10.1093/burnst/tkag040/8702856 by guest on 12 October 2026

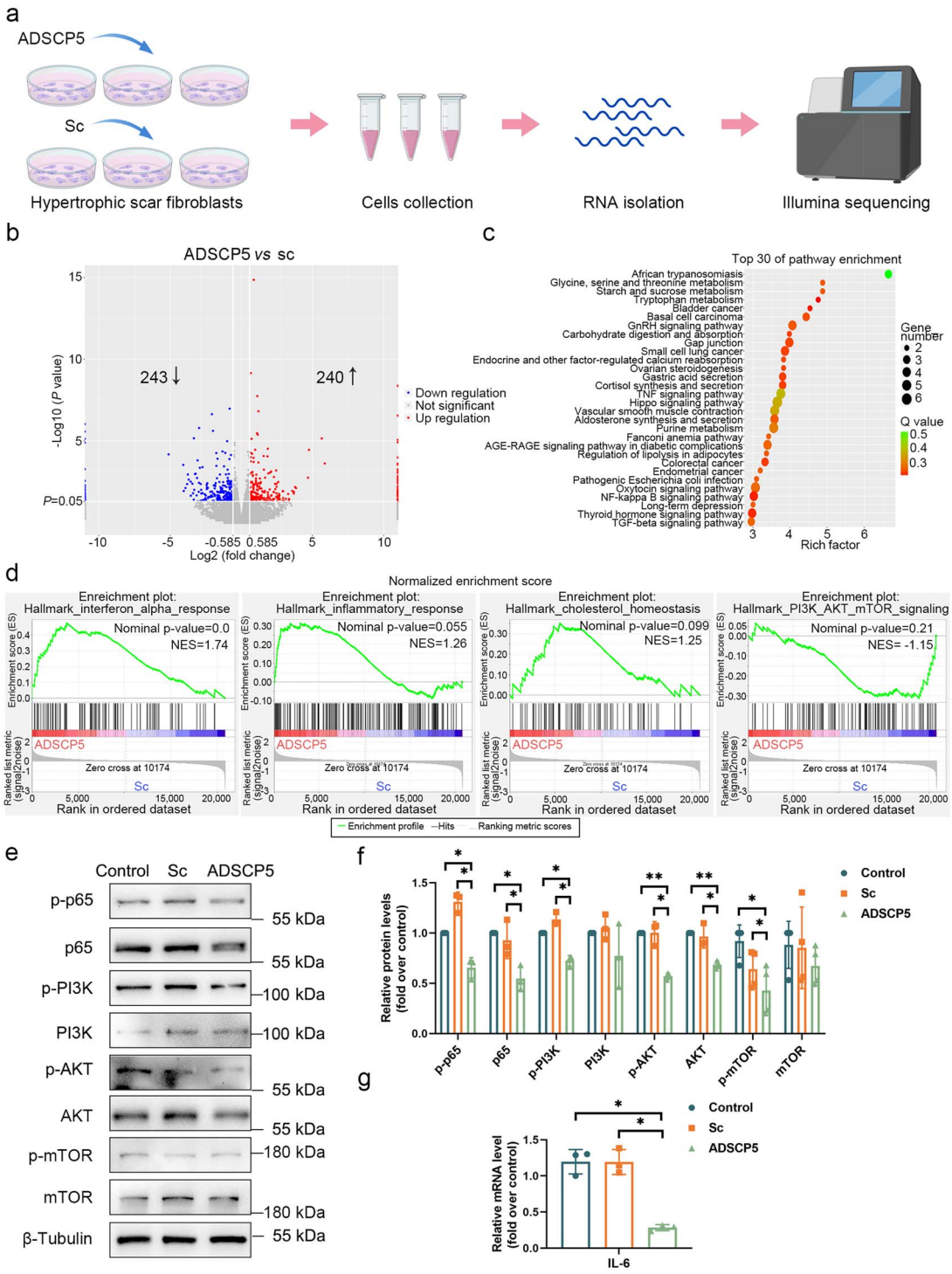



**Figure 2** The results of transcriptome sequencing suggest potential downstream mechanisms of ADSCP5. (**a**) Workflow of cellular RNA transcriptome sequencing. (**b**) Volcano plot of the differentially expressed genes. (**c**) KEGG pathway enrichment analysis of differentially expressed genes. (**d**) GSEA results. The NES represents the ES normalized by the mean of ES values from all randomly permuted gene sets. (**e**) Western blot analysis of p-p65, p65, p-PI3K, PI3K, and p-AKT protein levels. (**f**) Grayscale values of the western blot bands were analyzed using ImageJ software. (**g**) qPCR analysis of IL-6 expression in human hypertrophic scar-derived dermal fibroblasts treated with ADSCP5. GAPDH was used as the internal reference gene. Relative gene expression was calculated using the $2^{(-\Delta\Delta CT)}$ method. The data are presented as the mean ± SD from three or four independent experiments (n = 3 or 4). Protein or gene expression levels in the control group were normalized to 1. One-way ANOVA followed by Tukey's multiple comparisons test was used. $^{*}P < 0.05$, $^{**}P < 0.01$, $^{***}P < 0.001$. *ADSCP5* adipose-derived stem cell peptide 5, *Control* solvent control, *Sc* scrambled peptide control, *NES* normalized enrichment score, *p65* nuclear factor kappa B subunit p65, *PI3K* Phosphoinositide 3-kinase, *mTOR* mammalian target of rapamycin, *IL-6* interleukin-6

Downloaded from academic.oup.com/burnstrauma/article/doi/10.1093/burnst/tkag040/8702856 by guest on 12 October 2026

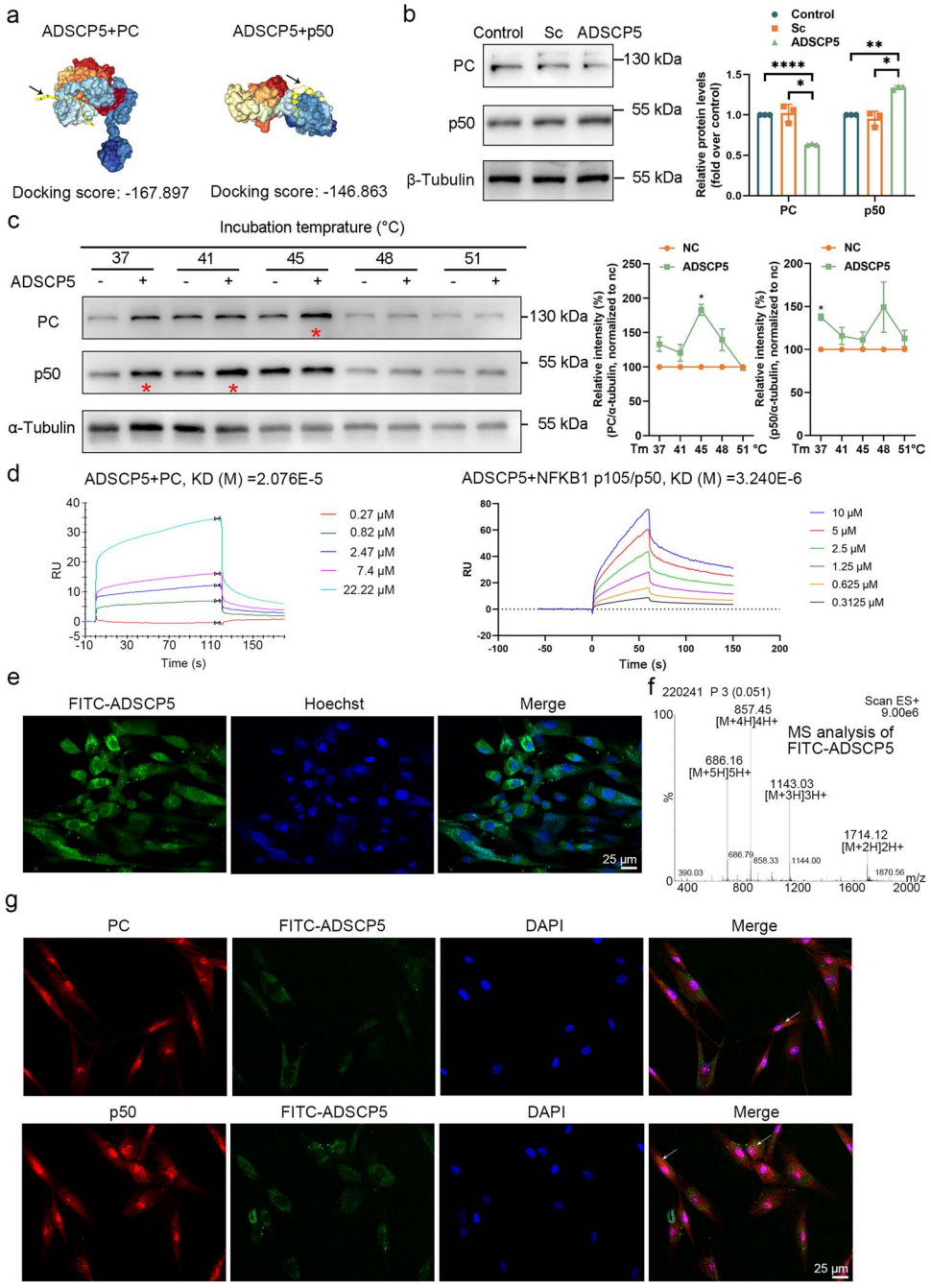



**Figure 3** Interaction between ADSCP5 and target proteins PC or p50. (**a**) Molecular docking analysis of ADSCP5 with PC and p50 proteins. (**b**) Western blot analysis demonstrating that ADSCP5 suppresses PC expression while promoting p50 expression. Grayscale analysis was performed using ImageJ software. The data are presented as the mean ± SD from three independent experiments ($n = 3$). Protein levels in the control group were normalized to 1. One-way ANOVA followed by Tukey's multiple comparisons test was used. $^{*}P < 0.05$, $^{**}P < 0.01$, $^{****}P < 0.0001$. (**c**) CETSA confirming the binding of ADSCP5 to PC and p50. Western blot results show protein degradation at increasing temperatures; stabilization of target proteins (reduced degradation) at identical temperatures indicates ligand binding. Grayscale analysis of western blot bands from CETSA was performed using ImageJ software. The data are presented as the mean ± standard error of the mean (SEM) from three independent experiments ($n = 3$). Protein expression levels in the NC group (CETSA) at each temperature were normalized to 100%. Two-way ANOVA followed by Sidak's multiple comparisons test was used. $^{*}P < 0.05$. (**d**) A representative SPR sensorgram was used to determine the interaction between PC or p50 and ADSCP5. (**e**) Subcellular location of FITC-labeled ADSCP5. (**f**) Mass spectrometry analysis of FITC-labeled ADSCP5. Scale bar: 25 $\mu$m. (**g**) Immunofluorescence staining of PC or p50 and colocalization with FITC-labeled ADSCP5 (white arrows). Scale bar: 25 $\mu$m. *ADSCP5* adipose-derived stem cell peptide 5, *Control* solvent control, *Sc* scrambled peptide control, *NC* negative control, solvent control, *PC* pyruvate carboxylase, *p50* nuclear factor kappa B subunit p50, *KD* dissociation constant, *RU* resonance units, *MS* mass spectrometry, *FITC* fluorescein isothiocyanate

Downloaded from academic.oup.com/burnstrauma/article/doi/10.1093/burnst/tkag040/8702856 by guest on 12 October 2026

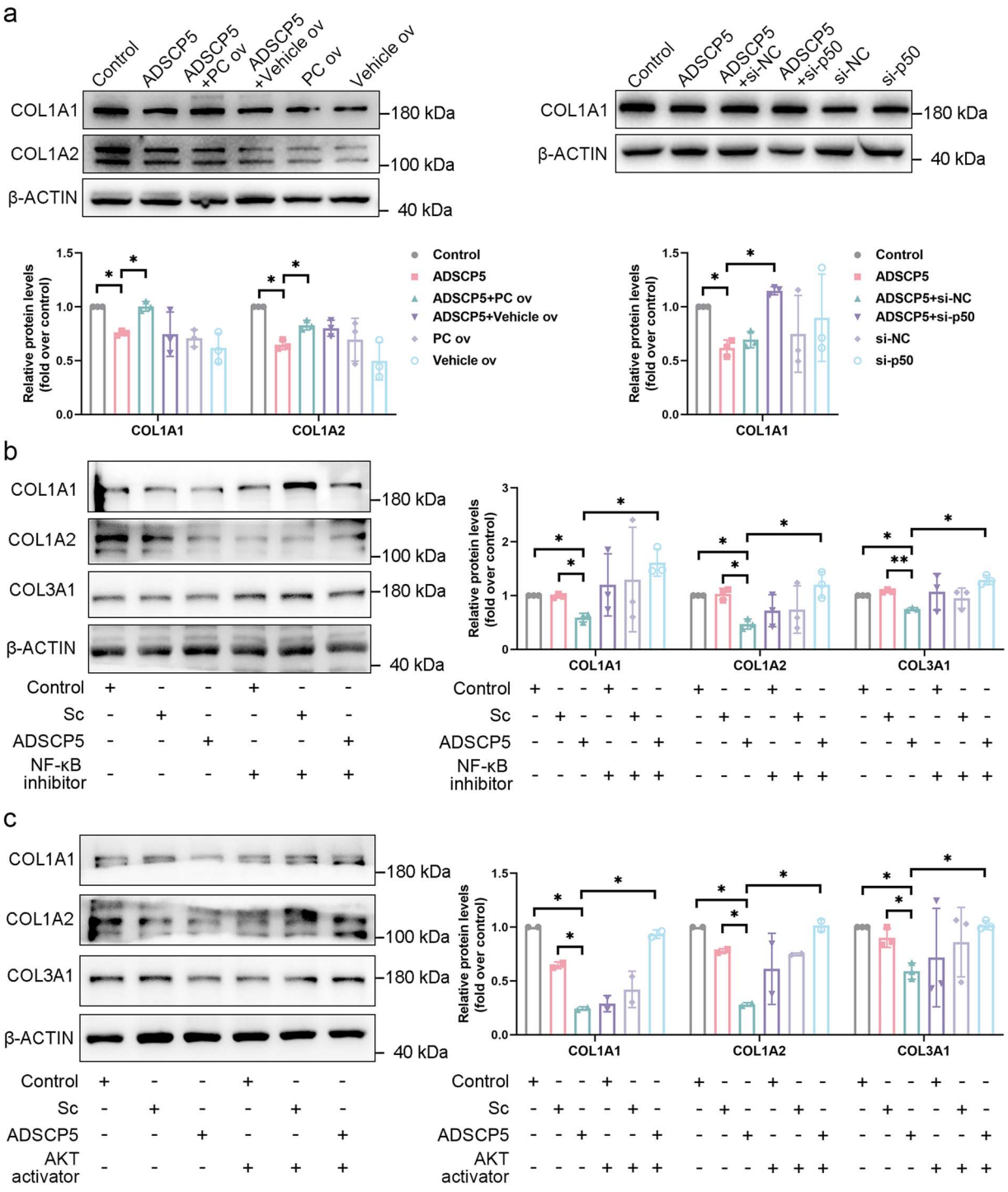



**Figure 4** Rescue experiments confirming that ADSCP5 functions through targeting PC or p50 and modulating the NF-$\kappa$B and AKT signaling pathways. (**a**) Western blot analysis of cells with overexpression of PC or knockdown of p50 for the rescue experiments. (**b**) Western blot analysis of the NF-$\kappa$B inhibitor rescue experiment. (**c**) Western blot analysis of the AKT activator rescue experiment. Grayscale values of western blot bands were analyzed using ImageJ software. The data are presented as the mean ± SD from three independent experiments ($n = 3$). The protein expression levels in the control group were normalized to 1. One-way ANOVA followed by Tukey's multiple comparisons test was used. $^{*}P < 0.05$, $^{**}P < 0.01$. *ADSCP5* adipose-derived stem cell peptide 5, *Control* solvent control, *Sc* scrambled peptide control, *si-NC* knochdown of negative control, *PC* pyruvate carboxylase

Downloaded from academic.oup.com/burnstrauma/article/doi/10.1093/burnst/tkag040/8702856 by guest on 12 October 2026

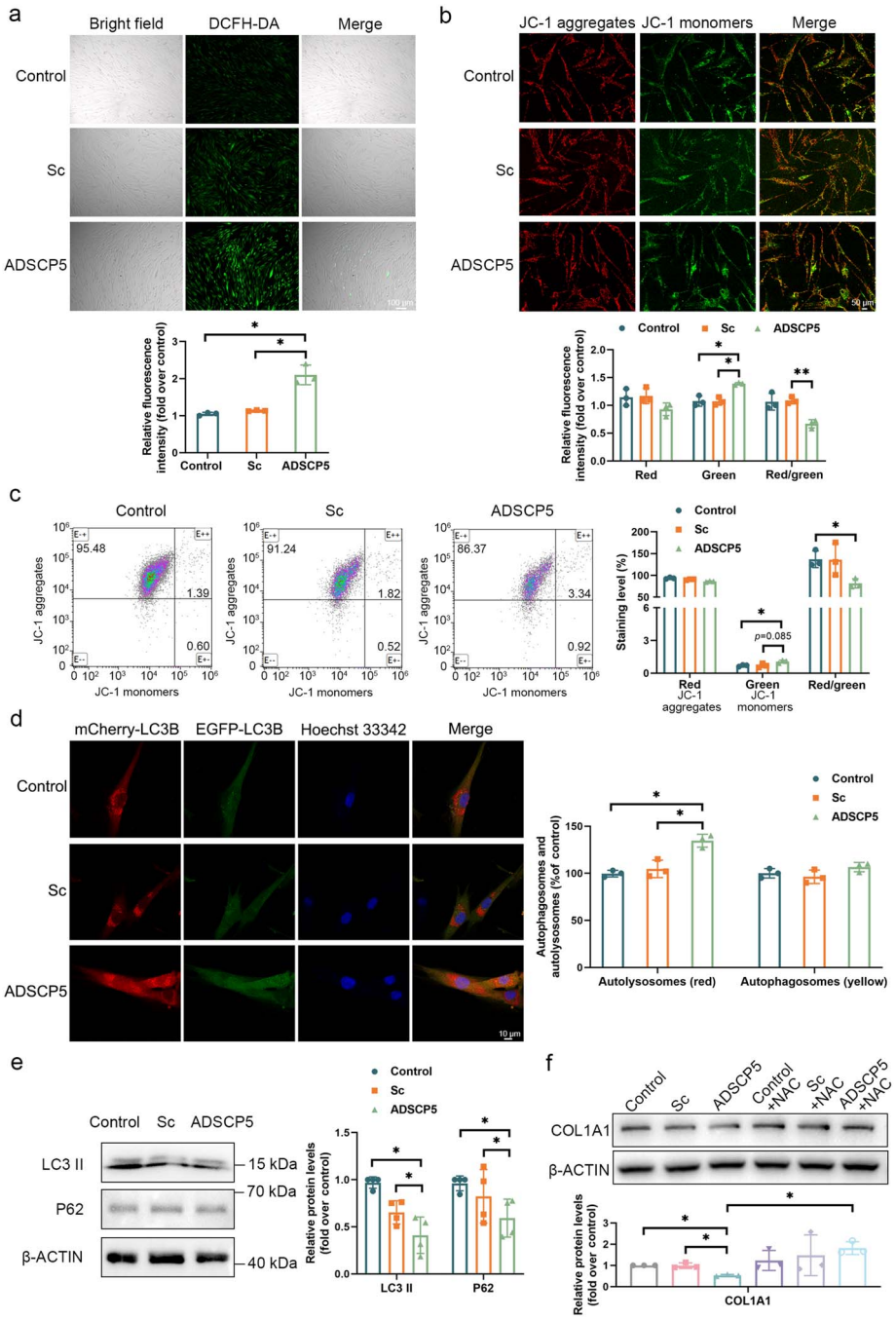



**Figure 5** Effects of ADSCP5 on ROS levels, mitochondrial membrane potential, autophagic flux, and autophagy-related protein expression in HSFs. (**a**) Measurement of intracellular ROS levels. The mean fluorescence intensity was quantified using ImageJ software. Scale bar: 100 $\mu$m. (**b**) JC-1 staining observed by Leica STELLARIS STED confocal microscopy: JC-1 aggregates (red fluorescence) indicate normal mitochondrial membrane potential, while JC-1 monomers (green fluorescence) indicate mitochondrial membrane depolarization. The data are presented as the mean ± SD from the mean fluorescence intensity per cell from 5 random fields and three independent experiments ($n = 3$). Scale bar: 50 $\mu$m. (**c**) Flow cytometry analysis of JC-1 staining. Statistical analysis of fluorescence signal percentages. (**d**) Fluorescence imaging using a Leica STELLARIS STED confocal microscopy system. Autophagic vesicles were characterized by merged fluorescence signals: mCherry single-positive/EGFP-negative puncta (red fluorescence) indicate autolysosomes, while mCherry/EGFP double-positive puncta (yellow fluorescence) indicate autophagosomes. Statistical analysis of autophagic flux. Changes were quantified by measuring the relative abundances of autolysosomes (red) and autophagosomes (yellow). Scale bar: 10 $\mu$m. (**e**) Western blot analysis of autophagy-related proteins. Grayscale analysis of the western blot bands was performed using ImageJ software. (**f**) Western blot analysis of the effects of NAC (a ROS scavenger). The data are presented as the mean ± SD from three or four independent experiments ($n = 3$ or 4). The mean fluorescence intensity in the control group for ROS detection or JC-1 staining was normalized to 1. The fluorescence intensity in the control group for autophagic flux was normalized to 100%, and the protein expression levels in the control group were normalized to 1. One-way ANOVA followed by Tukey's multiple comparisons test was used. $^{*}P < 0.05$, $^{**}P < 0.01$. *ADSCP5* adipose-derived stem cell peptide 5, *Control* solvent control, *Sc* scrambled peptide control

Downloaded from academic.oup.com/burnstrauma/article/doi/10.1093/burnst/tkag040/8702856 by guest on 12 October 2026

significantly disrupts multiple metabolic pathways, inhibiting the biosynthesis of key intermediates such as pyruvate, citrate, lactate, malate, aspartate, acetyl-CoA, and serine [24]. Therefore, hypertrophic scar fibroblasts were treated with 25 $\mu$M ADSCP5, and untargeted metabolomics analysis (Figure 6a) revealed 851 upregulated and 1012 downregulated metabolites (Figure 6b). A heatmap was constructed to visualize the expression profiles of differentially abundant metabolites across samples (Figure 6c). Z-score analysis revealed significant differences in metabolite levels between the control and ADSCP5-treated groups (Figure 6d). Enrichment analysis indicated predominant associations with purine and nucleotide metabolism (Figure 6e). The TCA cycle associated with PC protein is shown in Figure 6f. Several directly or indirectly related metabolites of PC protein exhibited upregulated or downregulated expression patterns (Figure 6f). The concurrent elevations in oxaloacetic acid and ADP levels suggest that following the ADSCP5-induced downregulation of PC protein expression, TCA cycle flux is impaired, triggering an energy crisis and the activation of compensatory anabolic pathways.

## ADSCP5-treated macrophages and HUVECs play roles in inhibiting collagen expression and promoting angiogenesis

Macrophages play a dual role in the formation and progression of hypertrophic scars, participating in both the proinflammatory injury phase and the regulation of the fibrotic repair process. Their mechanisms of action are complex and involve phenotypic polarization, cytokine secretion, and interactions with fibroblasts [25]. Therefore, this study further investigated the effects of ADSCP5 on macrophages. The morphological characteristics of RAW264.7 macrophages under microscopy are shown in Figure 7a.

After RAW264.7 macrophages were treated with ADSCP5, qPCR was performed to measure the mRNA expression levels of M1 (classically activated macrophages, proinflammatory)-related genes (CD86, CD80, iNOS, TNF-$\alpha$, IL-6, and IL-1) and M2 (alternatively activated macrophages, anti-inflammatory)-related genes (IL-10, CD206, CD204, Arg-1, and IL-4). IL-6 and CD206 mRNA expression levels were significantly lower in the ADSCP5 group than in the Sc group (Figure 7b). However, the expression levels of CD80, iNOS, TNF-$\alpha$, IL-10, CD204, and IL-4 did not significantly differ (Figure 7b). Furthermore, following ADSCP5 treatment, the culture supernatant of RAW264.7 macrophages was used to treat HSFs (Figure 7c). The mRNA expression levels of COL1A1, COL1A2, COL3A1, and ACTA2 were subsequently examined. Compared with the control or Sc-treated macrophage supernatant, the supernatant from ADSCP5-treated macrophages significantly suppressed the mRNA expression of COL1A1, COL1A2, COL3A1, and ACTA2 in hypertrophic scar fibroblasts (Figure 7c). Taken together, these findings revealed that the macrophages did not adopt a classical reparative M2 phenotype. Instead, they acquired a potent regulatory function, effectively suppressing scar-forming activity in fibroblasts. This functional antifibrotic reprogramming represents a more therapeutically relevant outcome than a mere shift in M1/M2 classification.

Angiogenesis is a critical pathophysiological process in both wound healing and the development of hypertrophic scarring; although early angiogenesis supports effective wound repair, excessive vascular proliferation is closely associated with scar hyperplasia [26]. In our study, treatment of HUVECs with 25 $\mu$M ADSCP5 resulted in a significant reduction in tube formation under Matrigel conditions when compared with Sc treatment (Figure 7d). These findings highlight the potential role of this peptide in inhibiting angiogenesis, suggesting that ADSCP5 may suppress hypertrophic scar formation.

## ADSCP5 alleviates hypertrophic scar formation in a rabbit ear scar model

To evaluate the effect of ADSCP5 on scar hyperplasia, we used a rabbit ear ventral hypertrophic scar model. The Sc peptide has been confirmed to be functionally inert and was used as the control. Both Sc and ADSCP5 (200 $\mu$M, 100 $\mu$l) were administered via local intradermal injection into the wound sites on rabbit ears. Wounds were created on Day 0 (D0). Peptide injections began 14 days later and were administered once weekly for a total of four injections. A blank control group was also included. Scar conditions were documented photographically on D14, D21, D28, and D35. Scar tissues were collected after imaging on D42 (Figure 8a). The results demonstrated that ADSCP5 treatment significantly inhibited scar hyperplasia (Figure 8b). Histological examination using H&E staining and Masson's trichrome staining revealed that ADSCP5 reduced collagen deposition (Figure 8c). Statistical analysis further confirmed that ADSCP5 significantly suppressed the scar areas on D28, D35, and D42 (Figure 8d).

Immunohistochemical analysis of angiogenesis-related proteins revealed that ADSCP5 suppressed the expression levels of both CD34 and VEGFA in rabbit ear scar tissue (Figure 8e). Concurrently, we evaluated the effects of ADSCP5 on the macrophage markers CD68 and CD206. Protein analysis revealed that ADSCP5 treatment significantly upregulated CD68 expression but downregulated CD206 expression (Figure 8e). Given that CD68 is a pan-macrophage marker, its increase indicates a general expansion of the macrophage population. This expansion, concomitant with the suppression of the M2-associated marker CD206 and the previously observed reduction in IL-6 mRNA (Figure 2g), suggests that ADSCP5 promotes a shift in macrophages toward a functionally restrained state, characterized by restricted inflammatory cytokine secretion despite an increase in cell number.

## Functional validation of ADSCP5 in a porcine dorsal hypertrophic scar model

Although the rabbit ear hypertrophic scar model is a classic system that is generally straightforward, with a scar phenotype similar to that of humans and avoiding interference from wound contraction, it has several limitations, including a long scar formation period (exceeding 28 days), the absence of skin appendages (i.e. sweat glands and hair follicles), and a lack of a mechanical tension microenvironment [27]. In contrast, the porcine dorsal scar model closely mimics human skin in terms of epidermal thickness, collagen arrangement, and appendage distribution, enabling the formation of human-like scar structures.

Therefore, we further established a porcine dorsal hypertrophic scar model that closely recapitulates the pathological features of human hypertrophic scarring. On Day 14, ADSCP5 (200 $\mu$M, 100 $\mu$l) or control solvent (200 $\mu$M, 100 $\mu$l) was intradermally injected into the scar tissue. Injections were repeated weekly for a total of four

Downloaded from academic.oup.com/burnstrauma/article/doi/10.1093/burnst/tkag040/8702856 by guest on 12 October 2026

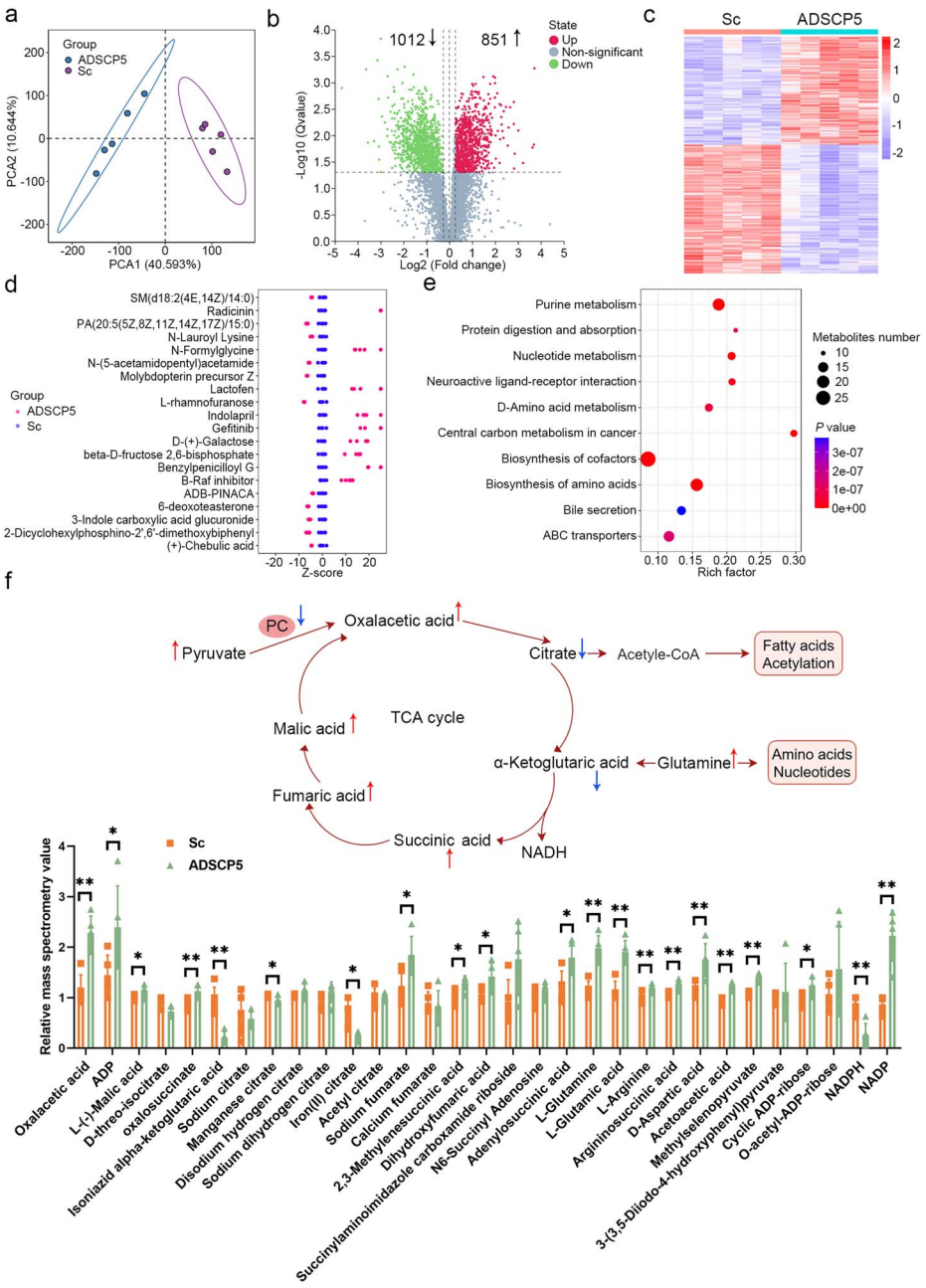



**Figure 6** Analysis of the impact of ADSCP5 on the metabolome of HSFs. (**a**) PCA score plot. The plot displays differences in metabolite composition among samples. PC1 and PC2 represent the first and second principal components, respectively, with the percentage of variance explained indicated in parentheses. The elliptical regions denote the 95% confidence intervals, and samples from different treatment groups are color-coded. (**b**) Screening of differentially abundant metabolites. Volcano plot visualization of differentially abundant metabolite expression. The x-axis shows the log2-fold change ($Log_2FC$), and the y-axis represents the significance level ($-Log_{10}Q$). Significantly upregulated (red) and downregulated (green) metabolites ($Q < 0.05$) are distributed outside the threshold lines; gray points indicate metabolites with no significant differences. (**c**) Expression patterns of differentially abundant metabolites. The heatmap illustrates the expression profiles of differentially abundant metabolites across samples. Rows represent metabolites, columns represent samples, and the color gradient (blue to red) indicates relative expression levels from low to high. Hierarchical clustering analysis reveals correlations between metabolite expression patterns and treatment conditions. (**d**) Z-score normalization analysis of metabolite relative abundance. The plot displays the intergroup differences in metabolite levels after Z-score normalization using the formula $z = (x-\mu)/\sigma$, where x is the measured value and $\mu$ and $\sigma$ are the mean and SD of the control group, respectively. Extreme values with $|Z\ score| > 20$ are shown at the axis boundaries. (**e**) Metabolic pathway enrichment analysis. The bubble plot shows significantly enriched metabolic pathways of differentially abundant metabolites. The x-axis represents the enrichment factor (number of differentially abundant metabolites/total metabolites in the pathway), the point size corresponds to the number of differentially abundant metabolites, and the color intensity indicates the significance level (*P* value). (**f**) Relative mass spectrometry values of different metabolites directly or indirectly associated with PC protein. The blue arrows indicate downregulated metabolites, and the red arrows indicate upregulated metabolites. *PCA* principal component analysis, *NADP* nicotinamide adenine dinucleotide phosphate, *NADPH* nicotinamide adenine dinucleotide phosphate, *ADP* adenosine diphosphate, *ADSCP5* adipose-derived stem cell peptide 5, *Control* solvent control, *Sc* scrambled peptide control

Downloaded from academic.oup.com/burnstrauma/article/doi/10.1093/burnst/tkag040/8702856 by guest on 12 October 2026

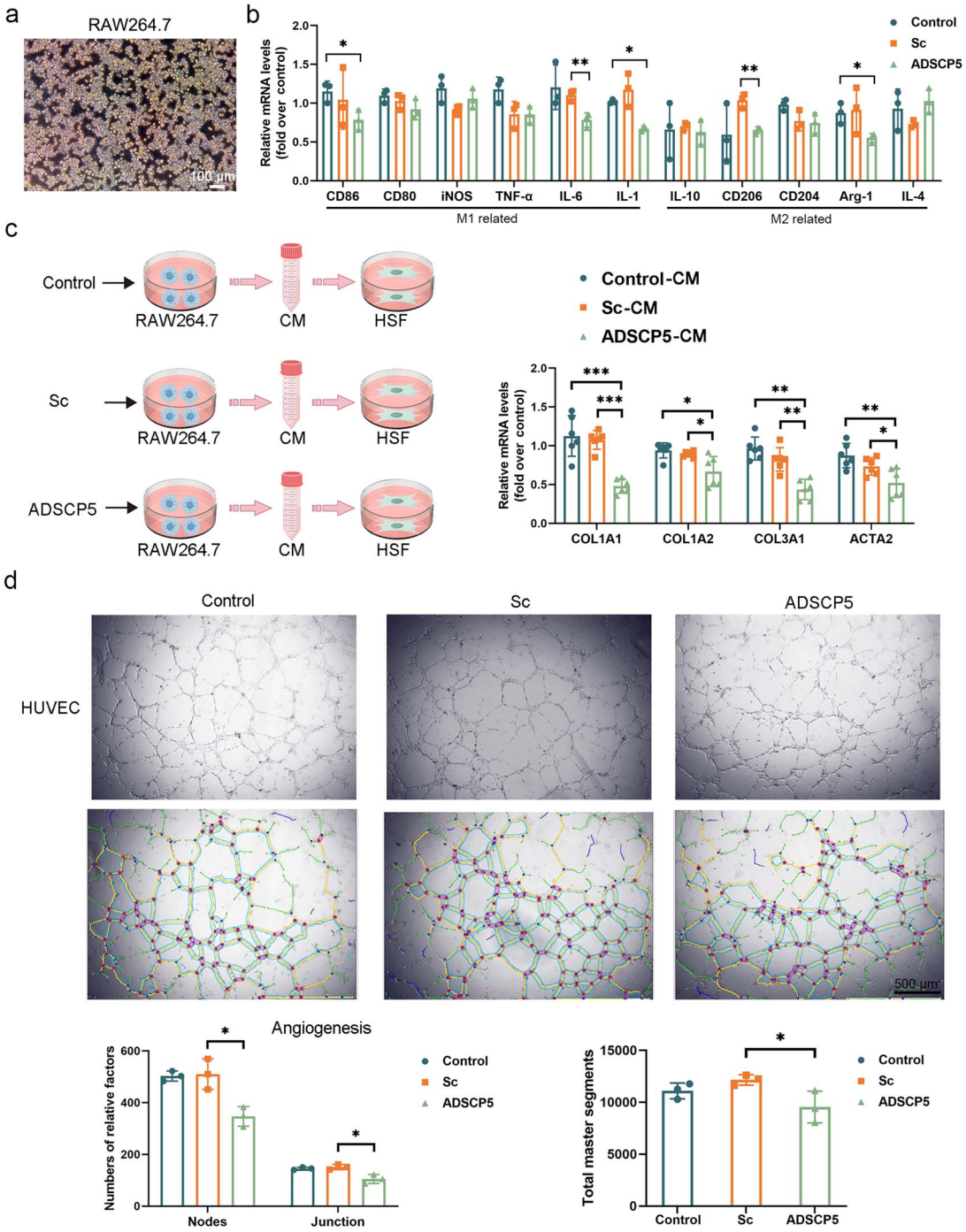



**Figure 7** Effects of ADSCP5 on macrophage polarization and its influence on collagen and ACTA2 expression in hypertrophic fibroblasts and angiogenesis in HUVECs. (**a**) Representative microscopy images showing the morphology of RAW264.7 macrophages. Scale bar: 100 $\mu$m. (**b**) qPCR analysis of M1/M2 macrophage polarization-related markers. (**c**) Schematic illustration of the experimental procedure: CM from peptide-treated macrophages was collected and applied to HSFs. qPCR analysis of collagen and ACTA2 mRNA expression in HSFs. The data are presented as the mean ± SD from three or six independent experiments ($n = 3$ or 6). Gene expression levels in the control or control-CM groups were normalized to 1. One-way ANOVA followed by Tukey's multiple comparisons test was used. $^{*}P < 0.05$, $^{**}P < 0.01$, $^{***}P < 0.001$. (**d**) Representative microscopy images of tube formation. Quantifications of tube length, covered area, number of loops, and number of junctions were performed using ImageJ software. Statistical analysis of tube formation parameters. Statistical significance between groups was determined using GraphPad Prism 8.0 software. The data are presented as the mean ± SD from three independent experiments ($n = 3$). One-way ANOVA followed by Tukey's multiple comparisons test was used. $^{*}P < 0.05$. Scale bar: 500 $\mu$m. *ADSCP5* adipose-derived stem cell peptide 5, *Control* solvent control, *Sc* scrambled peptide control, *NC* negative control, solvent control, *PC* pyruvate carboxylase, *HSF* hypertrophic scar fibroblasts, *CM* conditioned medium, iNOS inducible nitric oxide synthase, *TNF-α* tumor necrosis factor-alpha, *IL* interleukin

Downloaded from academic.oup.com/burnstrauma/article/doi/10.1093/burnst/tkag040/8702856 by guest on 12 October 2026

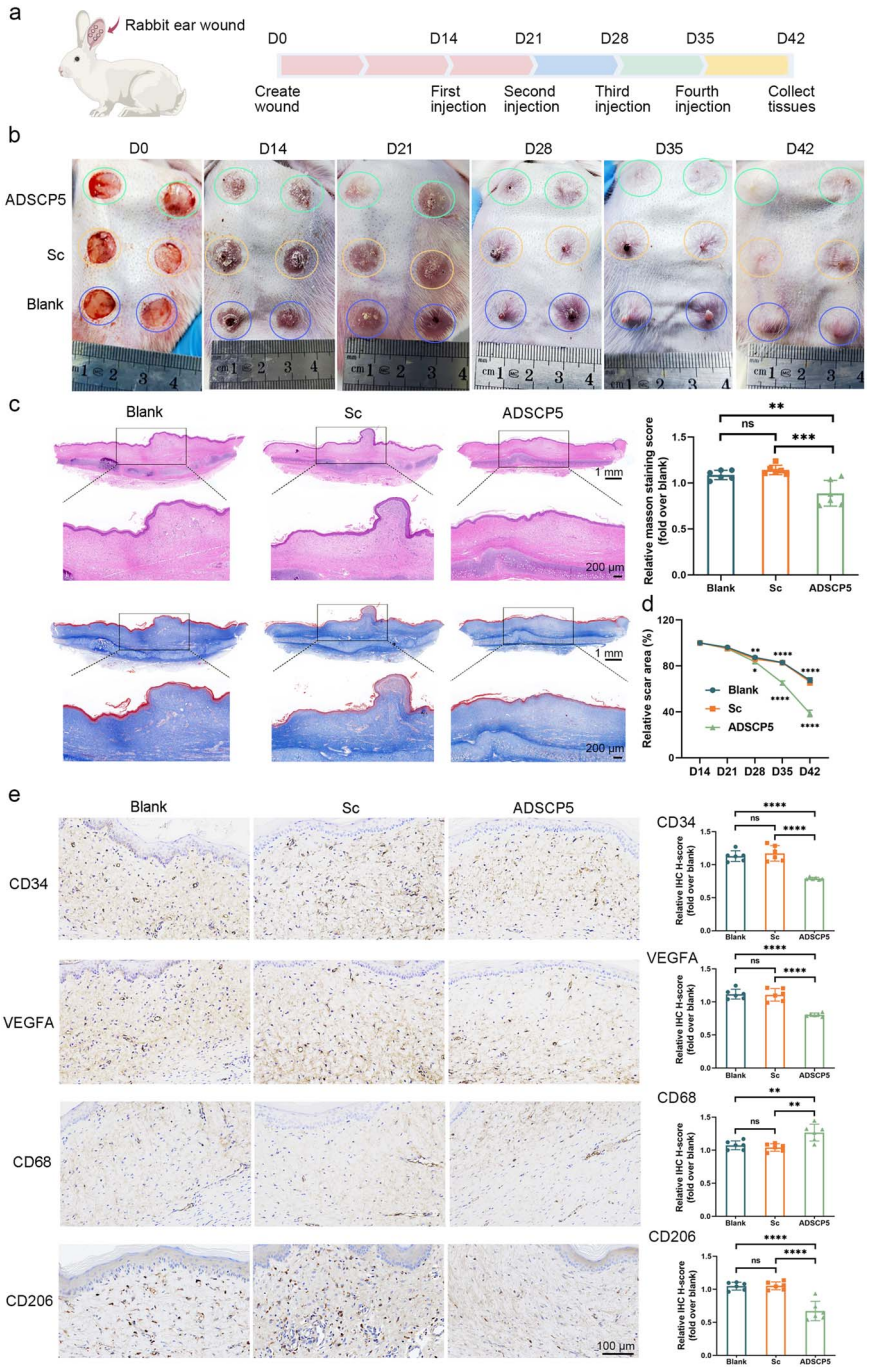



**Figure 8** ADSCP5 inhibits collagen synthesis and suppresses scar hyperplasia in a rabbit ear scar model, as determined by immunohistochemical analysis of the expression of CD34, VEGFA, CD68, and CD206 in rabbits. (**a**) Flowchart of the rabbit ear hypertrophic scar model. Six healthy New Zealand white rabbits were used in the study. Each rabbit received a total of 12 wounds (6 per year), which were divided into three groups: Blank, Sc, and ADSCP5, with 4 wounds per rabbit per group. (**b**) Representative photographs of wound healing. (**c**) H&E and Masson's trichrome staining analyses. Collagen deposition was quantitatively analyzed based on the Masson's trichrome staining intensity using ImageJ software. The staining intensity of one wound in the blank group was normalized to 1. The mean staining intensity from 4 wounds per rabbit was used to calculate the mean and SD. Scale bar: 1 mm; 200 $\mu$m. (**d**) Statistical analysis of the scar area measured using ImageJ software ($n = 6$). The scar area of one wound in the blank group was normalized to 100%. Two-way ANOVA followed by Tukey's multiple comparisons test was used. The asterisks above the line indicate comparisons between the control group and ADSCP5, and the asterisks below the line represent comparisons between the Sc group and ADSCP5. $^{*}P < 0.05$, $^{**}P < 0.01$, $^{****}P < 0.0001$. (**e**) CD34, VEGFA, CD68, and CD206 immunohistochemistry and staining intensity analysis ($n = 6$) were performed using ImageJ software. The staining intensity of one wound in the blank group was normalized to 1. One-way ANOVA followed by Tukey's multiple comparisons test was used. $^{**}P < 0.01$, $^{****}P < 0.0001$. Scale bar: 100 $\mu$m. *ADSCP5* adipose-derived stem cell peptide 5, *Sc* scrambled peptide control, *Blank* blank control

Downloaded from academic.oup.com/burnstrauma/article/doi/10.1093/burnst/tkag040/8702856 by guest on 12 October 2026

administrations, with photographic documentation throughout the process. Tissue samples were collected on Day 42 (Figure 9a). The photographic results revealed that the ADSCP5-treated group showed significant improvement in scar hyperplasia, characterized by reduced redness and swelling, yielding an appearance similar to that of normal tissue (Figure 9b, 9d). Statistical analysis confirmed that ADSCP5 significantly reduced the scar area on Days 28 and 35 (Figure 9c).

Scar tissue samples were subjected to H&E, Masson's trichrome, and Sirius red staining. The results revealed a significant reduction in collagen content in the ADSCP5-treated group (Figure 9e). Under polarized light microscopy, Sirius red staining further demonstrated marked decreases in both type III collagen (green birefringence) and type I collagen (yellow–red birefringence) (Figure 9f).

We collected porcine dorsal scar tissues treated with either control solvent or ADSCP5 and extracted the RNA for transcriptome sequencing. Volcano plots and cluster analyses of the DEGs are shown in Supplemental Figure 3a and 3b. Compared with the control treatment, ADSCP5 treatment resulted in 69 upregulated genes (fold change $>1.5$, $P < 0.05$) and 452 downregulated genes (fold change $\leq 0.67$, $P < 0.05$) (Supplemental Figure 3a). GO and KEGG pathway enrichment analyses of these 521 DEGs revealed significant associations with processes such as fatty acid biosynthesis (Supplemental Figure 3c, 3d). The top 30 upregulated and top 30 downregulated genes from the transcriptome sequencing results are listed in Tables 3 and 4, respectively.

Collected porcine dorsal scar tissues were analyzed via immunohistochemistry to evaluate the effect of ADSCP5 on the expression of the autophagy-related protein p62. The results revealed that ADSCP5 significantly suppressed p62 protein levels (Figure 9g), suggesting that the peptide enhances autophagy. Concurrently, changes in the macrophage marker CD68 were assessed, revealing a significant increase in CD68 protein levels following ADSCP5 treatment (Figure 9g).

# Discussion

Hypertrophic scarring is an abnormal tissue remodeling phenomenon that occurs during the wound healing process following injury to the dermal layer of the skin [2]. Recently, several studies have demonstrated that ADSCs play significant roles in suppressing pathological scar formation [5, 6]. Adipose-derived stem cells can effectively improve pathological scarring by mediating inflammation and regulating fibroblast proliferation and activation, and vascular reconstruction [28]. However, the safety, separation, and extraction standards of ADSCs need to be considered in clinical use. Peptide-based therapeutics hold great promise in disease treatment owing to their low molecular weight, high specificity, and low toxicity [9, 29]. Here, we demonstrate that the binding of ADSCP5 to PC inhibits PC enzymatic activity, leading to disruption of the TCA cycle and metabolic imbalance and reducing AKT/mTOR activity, which promotes autophagy. Simultaneously, metabolic imbalance leads to increased ROS levels. ROS can suppress PI3K/AKT signaling (which is consistent with reduced p-AKT levels). Decreased phosphorylation of AKT was accompanied by decreased phosphorylation of p65. Independently, the binding of ADSCP5 to p50 stabilized or increased p50 protein expression. The increase in p50 results in the formation of homodimers that translocate to the nucleus and repress the expression of NF-$\kappa$B-driven proinflammatory/profibrotic genes (including IL-6 and collagens). Importantly, ROS also promotes autophagy, which is further potentiated by AKT/mTOR inhibition, and autophagy has been shown to degrade collagen precursors. Thus, ADSCP5 alleviates hypertrophic scarring through targeting PC or p50 to coordinate PI3K/AKT/mTOR-autophagy and NF-$\kappa$B/IL-6 signaling. In addition, ADSCP5 may be considered a potential therapeutic agent for the prevention and treatment of pathological scarring.

PC, located in the mitochondria, catalyzes the conversion of pyruvate to oxaloacetate and thus supplies substrates for the TCA cycle. Pyruvate is a key intermediate in glucose metabolism and serves as a metabolic hub linking carbohydrate, lipid, and amino acid metabolism. Macrophage PC promotes inflammatory responses and exacerbates atherosclerosis via the HIF-1 signaling pathway [30]. A derivative of pulchinenoside B4 targets PC to treat ulcerative colitis [31]. Fibroblast PC in the tumor microenvironment is necessary for collagen production [32]. Our previous research revealed that the ADSC-derived ADSCP2 inhibits scarring by binding to PC and altering metabolite composition, and knockdown of PC decreased COL1A2, COL3A1, and ACTA2 protein levels [16]. Here, through peptide pull-down assays, mass spectrometry, molecular docking, cellular thermal shift assays (CETSAs), surface plasmon resonance, immunofluorescence colocalization analysis, and western blot and rescue experiments, we demonstrate that ADSCP5 binds to PC, inhibits its expression, and alters the metabolite profile of hypertrophic scar-derived fibroblasts via untargeted metabolomics.

Nuclear factor kappa B (NF-$\kappa$B) is a transcription factor widely expressed in eukaryotic cells that regulates genes involved in proliferation, differentiation, apoptosis, and fibrosis. The NF-$\kappa$B family includes RelA (p65), RelB, c-Rel, NF-$\kappa$B1 (p50), and NF-$\kappa$B2 (p52), which form homo- or heterodimers. The Rel homology domain (RHD) mediates dimerization, nuclear localization, DNA binding, and interaction with I$\kappa$B inhibitors [33]. Studies have shown that p50 homodimers act as key anti-inflammatory transcription factors by suppressing the expression of proinflammatory genes and increasing the expression of anti-inflammatory genes [34]. RNA-seq analysis revealed 483 genes whose expression differed after ADSCP5 treatment (Figure 2b). KEGG and GSEA analyses revealed associations with NF-$\kappa$B, interferon-alpha, the inflammatory response, cholesterol homeostasis, and the PI3K/AKT/mTOR pathway. We further confirmed that ADSCP5 binds p50 and promotes its expression. These findings suggest that ADSCP5 may facilitate p50 homodimer binding to the promoters of inflammatory genes such as IL-6 to suppress their transcription. Rescue experiments with a knockdown of p50 or an NF-$\kappa$B inhibitor attenuated ADSCP5-mediated suppression of COL1A1, indicating that ADSCP5 inhibits collagen via p50.

Protein kinase B (AKT) is a serine/threonine kinase. FAK activates the PI3K/AKT pathway to prevent fibroblast apoptosis, leading to fibroblast accumulation [35]. miR-203a-3p reduces hypertrophic scarring by inhibiting PI3K$\alpha$ via the PI3K/AKT/mTOR pathway [36]. Melatonin enhances autophagy through MT2 receptor-mediated PI3K/AKT/mTOR suppression, inhibiting fibroblast function and scarring [22]. Inhibiting ANGPT2 activates autophagy via the PI3K/AKT/mTOR pathway to regulate scarring [37]. We found that ADSCP5 inhibits AKT and mTOR expression, reduces p62 levels, and promotes autophagic flux. AKT activator treatment

Downloaded from academic.oup.com/burnstrauma/article/doi/10.1093/burnst/tkag040/8702856 by guest on 12 October 2026

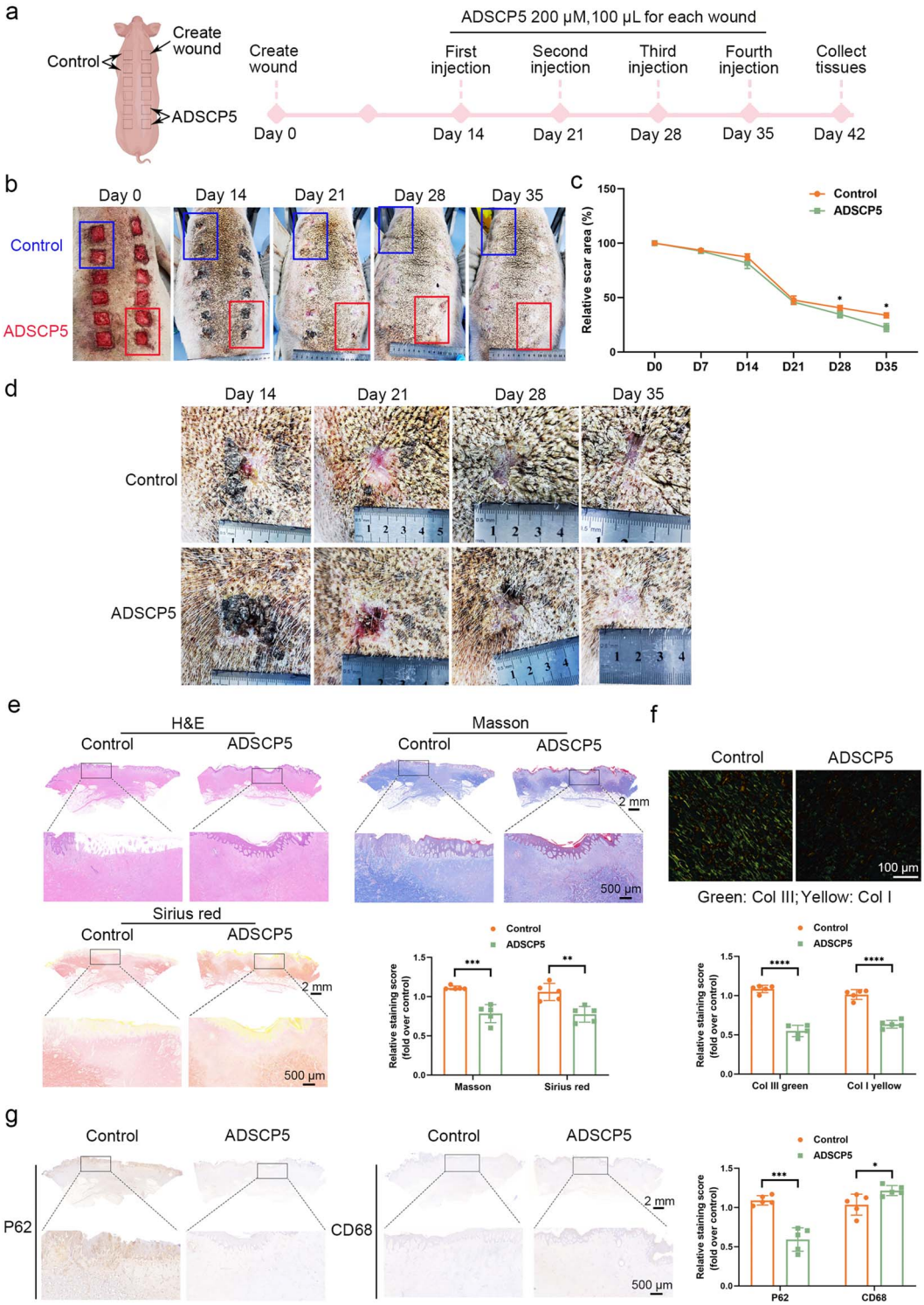



**Figure 9** Effects of ADSCP5 on hypertrophic scar formation, collagen deposition, and p62 and CD68 expression levels in a porcine dorsal skin model. (**a**) Flowchart of the wound healing model on porcine dorsal skin. Five Bama miniature pigs were used in the experiment, with two wounds assigned to the control group and two wounds to the ADSCP5 treatment group per pig. (**b**) Photographic documentation of wound healing on porcine dorsal skin. The blue boxes indicate the solvent control group, and the red boxes indicate the ADSCP5 group. (**c**) Statistical analysis of the scar area measured using ImageJ software. Each pig in each group had two wounds. The mean scar areas of each pig were used to calculate the mean and SD. The scar area of one wound in the control group was normalized to 100%. Two-way ANOVA followed by Sidak's multiple comparisons test was used. $^{*}P < 0.05$. (**d**) Enlarged views of the wound and scar areas. (**e**) H&E staining, Masson's trichrome staining, and Sirius red staining. Scale bar: 2 mm; 500 $\mu$m. (**f**) Polarized light imaging of Sirius red-stained sections: Green indicates type III collagen and yellow indicates type I collagen are indicated below the image. Scale bar: 100 $\mu$m. (**g**) Results from the immunohistochemistry analysis for p62 and CD68. Quantitative analysis of the staining intensities for collagen (Masson and Sirius red), p62, and CD68 was performed using ImageJ software. The mean staining intensity of each pig was used to calculate the mean and SD. The values in the control group were normalized to 1. An unpaired Student's *t*-test was employed. Scale bar: 2 mm; 500 $\mu$m. $^{*}P < 0.05$, $^{**}P < 0.01$, $^{***}P < 0.001$, $^{****}P < 0.0001$. *ADSCP5* adipose-derived stem cell peptide 5, *Control* solvent control, *H&E* hematoxylin–eosin staining

Downloaded from academic.oup.com/burnstrauma/article/doi/10.1093/burnst/tkag040/8702856 by guest on 12 October 2026

**Table 3** Top 30 upregulated genes after treatment with peptide adipose-derived stem cell peptide 5

| Gene name | Description | Log2 fold change | *P* value |
|---|---|---|---|
| ERICH6 | Glutamate rich 6 | 3.70 | 0.01 |
| CARD14 | Caspase recruitment domain family member 14 | 3.69 | 0.02 |
| DLGAP3 | DLG associated protein 3 | 3.58 | 0.01 |
| SIAH3 | Siah E3 ubiquitin protein ligase family member 3 | 3.36 | 0.04 |
| DHCR24-DT | DHCR24 divergent transcript | 3.30 | 0.02 |
| OVCH1 | Ovochymase 1 | 2.94 | 0.03 |
| PTPN20CP | Protein tyrosine phosphatase non-receptor type 20C, pseudogene | 2.91 | 0.05 |
| HAR1B | Highly accelerated region 1B | 2.72 | 0.04 |
| FIGURE NL2 | Fidgetin like 2 | 2.66 | 0.02 |
| ILDR2 | Immunoglobulin like domain containing receptor 2 | 2.66 | 0.03 |
| TGFB2-OT1 | TGFB2 overlapping transcript 1 | 2.59 | 0.00 |
| ATP6V1G3 | ATPase H+ transporting V1 subunit G3 | 2.57 | 0.02 |
| MCIDAS | Multiciliate differentiation and DNA synthesis associated cell cycle protein | 2.54 | 0.05 |
| CRHBP | Corticotropin releasing hormone binding protein | 2.48 | 0.01 |
| GRID1 | Glutamate ionotropic receptor delta type subunit 1 | 2.48 | 0.02 |
| FAM27E3 | Family with sequence similarity 27 member E3 | 2.46 | 0.03 |
| PCDHGA9 | Protocadherin gamma subfamily A, 9 | 2.45 | 0.00 |
| DUXAP8 | Double homeobox A pseudogene 8 | 2.31 | 0.04 |
| TDO2 | Tryptophan 2,3-dioxygenase | 2.27 | 0.04 |
| HSPA8P4 | Heat shock protein family A (Hsp70) member 8 pseudogene 4 | 2.25 | 0.04 |
| ZRSR2P1 | ZRSR2 pseudogene 1 | 2.10 | 0.00 |
| KLF17 | Kruppel-like factor 17 | 2.07 | 0.04 |
| PCDHGA3 | Protocadherin gamma subfamily A, 3 | 2.03 | 0.00 |
| FOXP3 | Forkhead box P3 | 2.00 | 0.01 |
| SULT1A2 | Sulfotransferase family 1A member 2 | 1.92 | 0.03 |
| ENPP3 | Ectonucleotide pyrophosphatase/phosphodiesterase 3 | 1.88 | 0.03 |
| PKD1L1 | Polycystin 1 like 1, transient receptor potential channel interacting | 1.87 | 0.02 |
| PCDHGA7 | Protocadherin gamma subfamily A, 7 | 1.86 | 0.00 |
| PLA2G4B | Phospholipase A2 group IVB | 1.84 | 0.00 |
| ZDHHC15 | Zinc finger DHHC-type palmitoyltransferase 15 | 1.67 | 0.00 |

reversed ADSCP5-mediated suppression of collagen expression, suggesting that ADSCP5 acts through AKT/mTOR inhibition and autophagy induction.

Autophagy is a highly regulated intracellular degradation process that maintains homeostasis through the recycling of damaged organelles and proteins via autophagosome–lysosome fusion [38]. It plays crucial roles in all phases of wound healing, inflammation, proliferation, and remodeling [39]. Autophagy impairment in hypertrophic scars hinders regression, limiting autophagy-mediated apoptosis and increasing ECM deposition [40]. Compared with normal skin, scar tissue has reduced levels of autophagy-related proteins (e.g. LC3-II and Beclin1) [41]. Enhancing autophagy may induce apoptosis and promote matrix degradation, offering a potential therapeutic strategy. A self-driving microneedle system (TA-Cur MNs) combined with autophagy modulation promotes scar repair [42].

During hypertrophic scarring, fibroblast overproliferation and microvascular occlusion create a hypoxic microenvironment, increasing ROS levels. Drug-loaded MNs can ameliorate the pathological microenvironment by scavenging ROS and reducing the MMP2/MMP9 ratio [43]. Surprisingly, ADSCP5 increased ROS production and partially reduced the mitochondrial membrane potential in human scar fibroblasts. Whereas autophagy typically reduces ROS accumulation by clearing ROS-related substrates, decreased PC expression may cause energetic stress, reducing AKT/mTOR activity and promoting autophagy. Thus, ADSCP5 may suppress PC, leading to metabolic dysregulation, partial mitochondrial depolarization, increased ROS levels, and increased autophagy.

Peptides often exert biological effects by binding target proteins and modulating their activity or conformation [44]. ADSCP5 may reduce PC levels by inducing conformational changes that

Downloaded from academic.oup.com/burnstrauma/article/doi/10.1093/burnst/tkag040/8702856 by guest on 12 October 2026

**Table 4** Top 30 downregulated genes after treatment with peptide adipose-derived stem cell peptide 5

| Gene name | Description | Log2 fold change | *P* value |
|---|---|---|---|
| HHIPL2 | HHIP like 2 | −3.80 | 0.00 |
| RIMBP3C | RIMS binding protein 3C | −3.75 | 0.00 |
| SOX30 | SRY-box transcription factor 30 | −3.39 | 0.02 |
| TRIM55 | Tripartite motif containing 55 | −3.34 | 0.04 |
| STARD6 | StAR related lipid transfer domain containing 6 | −3.31 | 0.01 |
| PRIMA1 | Proline rich membrane anchor 1 | −3.11 | 0.00 |
| PLLP | Plasmolipin | −3.06 | 0.05 |
| SOGA3 | SOGA family member 3 | −2.99 | 0.01 |
| TMEM59L | Transmembrane protein 59 like | −2.92 | 0.00 |
| KCNRG | Potassium channel regulator | −2.82 | 0.01 |
| MYC | MYC proto-oncogene, bHLH transcription factor | −2.73 | 0.00 |
| PKMP3 | Pyruvate kinase M1/2 pseudogene 3 | −2.71 | 0.02 |
| SOX18 | SRY-box transcription factor 18 | −2.61 | 0.04 |
| CLEC12A | C-type lectin domain family 12 member A | −2.52 | 0.04 |
| DOC2A | Double C2 domain alpha | −2.52 | 0.03 |
| KCP | Kielin cysteine-rich BMP regulator | −2.47 | 0.04 |
| CSF2 | Colony Stimulating Factor 2 | −2.43 | 0.00 |
| MMADHC-DT | MMADHC divergent transcript | −2.42 | 0.01 |
| DUSP15 | Dual specificity phosphatase 15 | −2.41 | 0.01 |
| TBC1D3 | TBC1 domain family member 3 | −2.41 | 0.01 |
| BHMT | Betaine—homocysteine S-methyltransferase | −2.33 | 0.03 |
| P2RY6 | Pyrimidinergic receptor P2Y6 | −2.17 | 0.01 |
| BEST4 | Bestrophin 4 | −2.14 | 0.03 |
| KCNJ15 | Potassium inwardly rectifying channel subfamily J member 15 | −2.06 | 0.00 |
| TEKT2 | Tektin 2 | −2.00 | 0.05 |
| SYNE4 | Spectrin repeat-containing nuclear envelope family member 4 | −1.96 | 0.05 |
| BEGAIN | Brain-enriched guanylate kinase associated | −1.93 | 0.01 |
| BATF | Basic leucine zipper ATF-like transcription factor | −1.92 | 0.05 |
| NUTM2E | NUT family member 2E | −1.88 | 0.02 |
| GFAP | Glial fibrillary acidic protein | −1.85 | 0.02 |

promote ubiquitin–proteasomal or autophagic–lysosomal degradation. Conversely, its binding to p50 may stabilize the protein and inhibit its degradation. The exact mechanisms require further validation. Overall, ADSCP5 appears to target PC or p50, although additional binding partners may exist.

Macrophages play dual roles in scarring, participating in both the proinflammatory and fibrotic phases via polarization, cytokine secretion, and fibroblast interactions [25]. Transdermal nanogels inhibit scarring by modulating macrophage polarization and exerting antifibrotic effects [45]. ADSCP5 treatment significantly reduced IL-6 mRNA expression in macrophages without affecting CD80, TNF-$\alpha$, CD204, or IL-4 expression. CM from ADSCP5-treated macrophages suppressed collagen and ACTA2 expression in fibroblasts. Because IL-6 overexpression promotes scarring, ADSCP5 may inhibit collagen and ACTA2 expression by reducing IL-6 secretion from macrophages.

Vascular endothelial cells contribute to scarring via angiogenesis, inflammation, transdifferentiation, and paracrine signaling [46]. Angiogenesis supplies oxygen and nutrients during healing; however, excessive angiogenesis can lead to scarring. ADSCP5 inhibited angiogenesis in HUVECs, suggesting a potential mechanism for its antiscarring effect, although further validation is needed.

Animal models for hypertrophic scarring include rabbit ear, mouse, rat, hamster, guinea pig, and pig models, each with advantages and limitations [27]. We demonstrated that ADSCP5 effectively suppressed collagen synthesis and scarring in both the rabbit ear and porcine back models. The rabbit ear model is simple and exhibits human-like scarring without wound contraction, but has a long formation period (>28 days) and lacks skin appendages and tension. Therefore, our assessments focused on histological and immunohistochemical markers of hypertrophy rather than biomechanical contraction metrics. The porcine model closely mimics human skin in structure and scarring but is costly and typically produces flat rather than raised scars. The porcine scars in this study were flat rather than raised, which may limit direct morphological comparison to elevated human hypertrophic scars. However, the model robustly captured the essential increase in

Downloaded from academic.oup.com/burnstrauma/article/doi/10.1093/burnst/tkag040/8702856 by guest on 12 October 2026

collagen pathology, making it suitable for evaluating antifibrotic therapeutics targeting collagen. In our study, the consistent results across the models underscore the conserved action of ADSCP5 and support its translational potential.

## Conclusions

Overall, this study demonstrates that ADSCP5 alleviates hypertrophic scarring by directly binding PC or p50, suppressing the PI3K/AKT/mTOR and NF-$\kappa$B pathways, and promoting ROS-mediated autophagy. By modulating metabolic, macrophage, and angiogenic responses, ADSCP5 effectively reduces collagen production and scar hyperplasia. These findings position ADSCP5 as a promising therapeutic agent for the prevention and treatment of pathological scarring, providing a theoretical basis for developing novel secretome-based anti-fibrotic strategies.

## Author contributions

Ling Chen (Conceptualization [equal], Formal analysis [lead], Funding acquisition [equal], Investigation [lead], Methodology [lead], Writing—original draft [lead]), Enyuan Zhang (Conceptualization [supporting], Formal analysis [supporting], Investigation [supporting], Methodology [supporting]), Siqi Zeng (Conceptualization [supporting], Formal analysis [supporting], Investigation [supporting]), Qiyue Yan (Formal analysis [supporting], Investigation [supporting], Methodology [supporting]), Jingyun Li (Conceptualization [supporting], Formal analysis [supporting], Funding acquisition [equal]), Qian Li (Formal analysis [supporting], Investigation [supporting], Methodology [supporting]), Jun Li (Conceptualization [equal], Formal analysis [equal], Funding acquisition [equal], Project administration [equal], Resources [equal], Supervision [equal], Writing—review & editing [equal]), and Zezhang Zhu (Conceptualization [equal], Formal analysis [equal], Funding acquisition [equal], Project administration [equal], Writing—review & editing [equal])

## Supplementary material

Supplementary material is available at *Burns & Trauma* online.

## Conflicts of interest

The authors declare that they have no conflicts of interest.

## Funding

This work was supported by National Natural Science Foundation of China (82472571, 82002041, 82072185), Jiangsu Provincial Medical Innovation Center of Orthopedic Surgery (CXZX202214), and Nanjing Medical Science and Technique Development Foundation (YKK21164, YKK24145). The funders had no role in the study design, data collection and analysis, decision to publish, or preparation of the manuscript.

## Data availability

The data that support the findings of this study are available from the corresponding author upon reasonable request.

## Ethics approval and consent to participate

This study was approved by the Ethics Committee of Women's Hospital of Nanjing Medical University (Nanjing Women and Children's Healthcare Hospital) (2022KY-162). Human hypertrophic scar tissues were obtained with written informed consent from patients undergoing surgery.

All the rabbit procedures were approved by the Experimental Animal Care and Use Committee (FJABR2022062201), and all the pig procedures were approved by the Experimental Animal Care and Use Committee (FJABR2022122901) and complied with the NIH guidelines.

## References

1. Fang X, Wang Y, Chen H, Yan Z, Jin S, Wu Y, *et al.* Hypertrophic scarring and keloids: epidemiology, molecular pathogenesis, and therapeutic interventions. *MedComm* (2020). 2025;6:e70381. https://doi.org/10.1002/mco2.70381
2. Pena OA, Martin P. Cellular and molecular mechanisms of skin wound healing. *Nat Rev Mol Cell Biol* 2024;25:599–616. https://doi.org/10.1038/s41580-024-00715-1
3. Jeschke MG, Wood FM, Middelkoop E, Bayat A, Teot L, Ogawa R, *et al.* Scars. *Nat Rev Dis Primers* 2023;9:64. https://doi.org/10.1038/s41572-023-00474-x
4. Mony MP, Harmon KA, Hess R, Dorafshar AH, Shafikhani SH. An updated review of hypertrophic scarring. *Cells.* 2023;12:12. https://doi.org/10.3390/cells12050678
5. Suh A, Pham A, Cress MJ, Pincelli T, TerKonda SP, Bruce AJ, *et al.* Adipose-derived cellular and cell-derived regenerative therapies in dermatology and aesthetic rejuvenation. *Ageing Res Rev* 2019;54:100933. https://doi.org/10.1016/j.arr.2019.100933
6. Borovikova AA, Ziegler ME, Banyard DA, Wirth GA, Paydar KZ, Evans GRD. *et al.* Adipose-derived tissue in the treatment of dermal fibrosis: antifibrotic effects of adipose-derived stem cells. *Ann Plast Surg* 2018;80:297–307. https://doi.org/10.1097/SAP.0000000000001278
7. Li Y, Zhang W, Gao J, Liu J, Wang H, Li J, *et al.* Adipose tissue-derived stem cells suppress hypertrophic scar fibrosis via the p38/mapk signaling pathway. *Stem Cell Res Ther* 2016;7:102. https://doi.org/10.1186/s13287-016-0356-6
8. Mazini L, Rochette L, Admou B, Amal S, Malka G. Hopes and limits of adipose-derived stem cells (adscs) and mesenchymal stem cells (mscs) in wound healing. *Int J Mol Sci* 2020;21:21. https://doi.org/10.3390/ijms21041306
9. Sharma K, Sharma KK, Sharma A, Jain R. Peptide-based drug discovery: current status and recent advances. *Drug Discov Today* 2023;28:103464. https://doi.org/10.1016/j.drudis.2022.103464
10. Song J, Li X, Li J. Emerging evidence for the roles of peptide in hypertrophic scar. *Life Sci* 2020;241:117174. https://doi.org/10.1016/j.lfs.2019.117174
11. Wang L, Fu Z, Su Y, Yin W, Wang X, Zhao W, *et al.* Cyclic heptapeptide fz1 acts as an integrin alphavbeta3 agonist to facilitate diabetic skin wound healing by enhancing angiogenesis. *J Med Chem* 2025;68:19503–20. https://doi.org/10.1021/acs.jmedchem.5c01734

Downloaded from academic.oup.com/burnstrauma/article/doi/10.1093/burnst/tkag040/8702856 by guest on 12 October 2026

12. Ru ZQ, Wu YT, Yang CY, Yang YT, Li YJ, Liu M, *et al.* Ultra-short cyclic peptide cy (rl-qn15) acts as a tlr4 antagonist to expedite oral ulcer healing. *Zool Res* 2025;46:1187–202. https://doi.org/10.24272/j.issn.2095-8137.2025.211
13. Wu YT, Ru ZQ, Peng Y, Fu Z, Jia QY, Kang ZJ, *et al.* Peptide cy (rl-qn15) accelerates hair regeneration in diabetic mice by binding to the frizzled-7 receptor. *Zool Res* 2024;45:1287–99. https://doi.org/10.24272/j.issn.2095-8137.2024.134
14. Jia Q, Fu Z, Li Y, Kang Z, Wu Y, Ru Z, *et al.* Hydrogel loaded with peptide-containing nanocomplexes: symphonic cooperation of photothermal antimicrobial nanoparticles and prohealing peptides for the treatment of infected wounds. *ACS Appl Mater Interfaces* 2024;16:13422–38. https://doi.org/10.1021/acsami.3c16061
15. Li C, Xiong Y, Fu Z, Ji Y, Yan J, Kong Y, *et al.* The direct binding of bioactive peptide andersonin-w1 to tlr4 expedites the healing of diabetic skin wounds. *Cell Mol Biol Lett* 2024;29:24. https://doi.org/10.1186/s11658-024-00542-4
16. Li J, Yin Y, Zou J, Zhang E, Li Q, Chen L, *et al.* The adipose-derived stem cell peptide adscp2 alleviates hypertrophic scar fibrosis via binding with pyruvate carboxylase and remodeling the metabolic landscape. *Acta Physiol (Oxf)* 2023;238:e14010. https://doi.org/10.1111/apha.14010
17. Lamiable A, Thevenet P, Rey J, Vavrusa M, Derreumaux P, Tuffery P. Pep-fold3: faster de novo structure prediction for linear peptides in solution and in complex. *Nucleic Acids Res* 2016;44:W449–54. https://doi.org/10.1093/nar/gkw329
18. Ray S, Ju X, Sun H, Finnerty CC, Herndon DN, Brasier AR. The il-6 trans-signaling-stat3 pathway mediates ecm and cellular proliferation in fibroblasts from hypertrophic scar. *J Invest Dermatol* 2013;133:1212–20. https://doi.org/10.1038/jid.2012.499
19. Shao Y, Guo Z, Yang Y, Liu L, Huang J, Chen Y. *et al.* Neutrophil extracellular traps contribute to myofibroblast differentiation and scar hyperplasia through the toll-like receptor 9/nuclear factor kappa-b/interleukin-6 pathway. *Burns Trauma* 2022;10:tkac044. https://doi.org/10.1093/burnst/tkac044
20. Wilmanski T, Zhou X, Zheng W, Shinde A, Donkin SS, Wendt M, *et al.* Inhibition of pyruvate carboxylase by 1alpha,25-dihydroxyvitamin d promotes oxidative stress in early breast cancer progression. *Cancer Lett* 2017;411:171–81. https://doi.org/10.1016/j.canlet.2017.09.045
21. Li J, Zeng S, Sun Y, Zou J, Zhang E, Yan Q, *et al.* Gluconic acid alleviates hypertrophic scar formation through binding plod1, reducing p-akt signaling and activating autophagy. *Phytomedicine.* 2025;143:156825. https://doi.org/10.1016/j.phymed.2025.156825
22. Dong Y, Cao X, Huang J, Hu Z, Chen C, Chen M, *et al.* Melatonin inhibits fibroblast cell functions and hypertrophic scar formation by enhancing autophagy through the mt2 receptor-inhibited pi3k/akt /mtor signaling. *Biochim Biophys Acta Mol basis Dis* 2024;1870:166887. https://doi.org/10.1016/j.bbadis.2023.166887
23. Lopez-Alonso JP, Lazaro M, Gil-Carton D, Choi PH, Dodu A, Tong L, *et al.* Cryoem structural exploration of catalytically active enzyme pyruvate carboxylase. *Nat Commun* 2022;13:6185. https://doi.org/10.1038/s41467-022-33987-2
24. Phannasil P, Ansari IH, El Azzouny M, Longacre MJ, Rattanapornsompong K, Burant CF, *et al.* Mass spectrometry analysis shows the biosynthetic pathways supported by pyruvate carboxylase in highly invasive breast cancer cells. *Biochim Biophys Acta Mol basis Dis* 2017;1863:537–51. https://doi.org/10.1016/j.bbadis.2016.11.021
25. Xu X, Gu S, Huang X, Ren J, Gu Y, Wei C, *et al.* The role of macrophages in the formation of hypertrophic scars and keloids. *Burns Trauma* 2020;8:tkaa006. https://doi.org/10.1093/burnst/tkaa006
26. Korntner S, Lehner C, Gehwolf R, Wagner A, Grutz M, Kunkel N, *et al.* Limiting angiogenesis to modulate scar formation. *Adv Drug Deliv Rev* 2019;146:170–89. https://doi.org/10.1016/j.addr.2018.02.010
27. Li J, Wang J, Wang Z, Xia Y, Zhou M, Zhong A, *et al.* Experimental models for cutaneous hypertrophic scar research. *Wound Repair Regen* 2020;28:126–44. https://doi.org/10.1111/wrr.12760
28. Wang M, Zhao J, Li J, Meng M, Zhu M. Insights into the role of adipose-derived stem cells and secretome: potential biology and clinical applications in hypertrophic scarring. *Stem Cell Res Ther* 2024;15:137. https://doi.org/10.1186/s13287-024-03749-6
29. Wang M, Xia H, Wang C, Zhang T, Zhang M, Li X, *et al.* From precision synthesis to cross-industry applications: the future of emerging peptide technologies. *Pharmacol Res* 2025;218:107839. https://doi.org/10.1016/j.phrs.2025.107839
30. Zhao LN, Wang RL, Liu RX, Zheng MR, Zhao L, Li BF, *et al.* Pyruvate carboxylase in macrophages aggravates atherosclerosis by regulating metabolism reprogramming to promote inflammatory responses through the hypoxia-inducible factor-1 signaling pathway. *Adv Sci (Weinh)* 2025;12:e17128. https://doi.org/10.1002/advs.202417128
31. Lv L, Li Q, Wang K, Zhao J, Deng K, Zhang R, *et al.* Discovery of a new anti-inflammatory agent from anemoside b4 derivatives and its therapeutic effect on colitis by targeting pyruvate carboxylase. *J Med Chem* 2024;67:7385–405. https://doi.org/10.1021/acs.jmedchem.4c00222
32. Schworer S, Pavlova NN, Cimino FV, King B, Cai X, Sizemore GM, *et al.* Fibroblast pyruvate carboxylase is required for collagen production in the tumour microenvironment. *Nat Metab* 2021;3:1484–99. https://doi.org/10.1038/s42255-021-00480-x
33. Mao H, Zhao X, Sun SC. Nf-kappab in inflammation and cancer. *Cell Mol Immunol* 2025;22:811–39. https://doi.org/10.1038/s41423-025-01310-w
34. Cartwright T, Perkins ND, C LW. Nfkb1: a suppressor of inflammation, ageing and cancer. *FEBS J* 2016;283:1812–22. https://doi.org/10.1111/febs.13627
35. Zhao S, Liu H, Wang H, He X, Tang J, Qi S, *et al.* Inhibition of phosphatidylinositol 3-kinase catalytic subunit alpha by mir-203a-3p reduces hypertrophic scar formation via phosphatidylinositol 3-kinase/akt/mtor signaling pathway. *Burns Trauma* 2024;12:tkad048. https://doi.org/10.1093/burnst/tkad048
36. Zhao S, Kong H, Qi D, Qiao Y, Li Y, Cao Z, *et al.* Epidermal stem cell derived exosomes-induced dedifferentiation of myofibroblasts inhibits scarring via the mir-203a-3p/pik3ca axis. *J Nanobiotechnology* 2025;23:56. https://doi.org/10.1186/s12951-025-03157-9
37. Chen H, Xu K, Sun C, Gui S, Wu J, Wang S. Inhibition of angpt2 activates autophagy during hypertrophic scar formation via


Downloaded from academic.oup.com/burnstrauma/article/doi/10.1093/burnst/tkag040/8702856 by guest on 12 October 2026

pi3k/akt/mtor pathway. *An Bras Dermatol* 2023;98:26–35. https://doi.org/10.1016/j.abd.2021.12.005

38. Dikic I, Elazar Z. Mechanism and medical implications of mammalian autophagy. *Nat Rev Mol Cell Biol* 2018;19:349–64. https://doi.org/10.1038/s41580-018-0003-4
39. Mijaljica D, Spada F, Klionsky DJ, Harrison IP. Autophagy is the key to making chronic wounds acute in skin wound healing. *Autophagy.* 2023;19:2578–84. https://doi.org/10.1080/15548627.2023.2194155
40. Sylakowski K, Wells A. Ecm-regulation of autophagy: the yin and the yang of autophagy during wound healing. *Matrix Biol* 2021;100-101:197–206. https://doi.org/10.1016/j.matbio.2020.12.006
41. Shi JH, Hu DH, Zhang ZF, Bai XZ, Wang HT, Zhu XX, *et al.* Reduced expression of microtubule-associated protein 1 light chain 3 in hypertrophic scars. *Arch Dermatol Res* 2012;304:209–15. https://doi.org/10.1007/s00403-012-1204-x
42. Wen T, Fu Y, Yi X, Sun Y, Zhao W, Shi C, *et al.* Autonomous drug delivery and scar microenvironment remodeling using micromotor-driven microneedles for hypertrophic scars therapy. *Acta Pharm Sin B* 2025;15:3738–55. https://doi.org/10.1016/j.apsb.2025.05.017
43. Yang ZR, Suo H, Fan JW, Lv N, Du K, Ma T, *et al.* Endogenous stimuli-responsive separating microneedles to inhibit hypertrophic scar through remodeling the pathological microenvironment. *Nat Commun* 2024;15:2038. https://doi.org/10.1038/s41467-024-46328-2
44. Petsalaki E, Russell RB. Peptide-mediated interactions in biological systems: new discoveries and applications. *Curr Opin Biotechnol* 2008;19:344–50. https://doi.org/10.1016/j.copbio.2008.06.004
45. Chen Y, Chen K, Zhong S, Wang J, Yu Z, Sun X, *et al.* Transdermal transfersome nanogels control hypertrophic scar formation via synergy of macrophage phenotype-switching and anti-fibrosis effect. *Adv Sci (Weinh)* 2024;11:e2305468. https://doi.org/10.1002/advs.202305468
46. Tan Y, Zhang M, Kong Y, Zhang F, Wang Y, Huang Y, *et al.* Fibroblasts and endothelial cells interplay drives hypertrophic scar formation: insights from in vitro and in vivo models. *Bioeng Transl Med* 2024;9:e10630. https://doi.org/10.1002/btm2.10630

Downloaded from academic.oup.com/burnstrauma/article/doi/10.1093/burnst/tkag040/8702856 by guest on 12 October 2026

© The Author(s) 2026. Published by Oxford University Press. This is an Open Access article distributed under the terms of the Creative Commons Attribution-NonCommercial License (https://creativecommons.org/licenses/by-nc/4.0/), which permits non-commercial re-use, distribution, and reproduction in any medium, provided the original work is properly cited. For commercial re-use, please contact reprints@oup.com for reprints and translation rights for reprints. All other permissions can be obtained through our RightsLink service via the Permissions link on the article page on our site—for further information please contact journals.permissions@oup.com.
*Burns & Trauma*, 2026, 14, tkag040
https://doi.org/10.1093/burnst/tkag040
Research Article